Astronomy & Astrophysics manuscript no. quartet
August 23, 2011
© ESO 2011

arXiv:1108.4349v1 [astro-ph.GA] 22 Aug 2011

Constraining Galactic cosmic-ray parameters with $Z \leq 2$ nuclei

B. Coste[1], L. Derome[1], D. Maurin[1], and A. Putze[2]

[1] Laboratoire de Physique Subatomique et de Cosmologie, Université Joseph Fourier Grenoble 1, CNRS/IN2P3, Institut Polytechnique de Grenoble, 53 avenue des Martyrs, Grenoble, 38026, France
[2] The Oskar Klein Centre for Cosmoparticle Physics, Department of Physics, Stockholm University, AlbaNova, SE-10691 Stockholm, Sweden

Received / Accepted

ABSTRACT

Context. The secondary-to-primary B/C ratio is widely used to study Galactic cosmic-ray propagation processes. The ^{2}H/^{4}He and ^{3}He/^{4}He ratios probe a different Z/A regime, therefore testing the 'universality' of propagation.
Aims. We revisit the constraints on diffusion-model parameters set by the quartet (^{1}H,^{2}H,^{3}He,^{4}He), using the most recent data as well as updated formulae for the inelastic and production cross-sections.
Methods. The analysis relies on the USINE propagation package and a Markov Chain Monte Carlo technique to estimate the probability density functions of the parameters. Simulated data are also used to validate analysis strategies.
Results. The fragmentation of CNO cosmic rays (resp. NeMgSiFe) on the ISM during their propagation contributes to 20% (resp. 20%) of the ^{2}H and 15% (resp. 10%) of the ^{3}He flux at high energy. The C to Fe elements are also responsible for up to 10% of the ^{4}He flux measured at 1 GeV/n. The analysis of ^{3}He/^{4}He (and to a less extent ^{2}H/^{4}He) data shows that the transport parameters are consistent with those from the B/C analysis: the diffusion model with $\delta \sim 0.7$ (diffusion slope), $V_c \sim 20$ km s^{-1} (galactic wind), $V_a \sim 40$ km s^{-1} (reacceleration) is favoured, but the combination $\delta \sim 0.2$, $V_c \sim 0$, and $V_a \sim 80$ km s^{-1} is a close second. The confidence intervals on the parameters show that the constraints set by the quartet data are competitive with those brought by the B/C data. These constraints are tighter when adding the ^{3}He (or ^{2}H) flux measurements, and the tightest when further adding the He flux. For the latter, the analysis of simulated and real data show an increased sensitivity to biases. Using secondary-to-primary ratio along with a loose prior on the source parameters is recommended to get the most robust constraints on the transport parameters.
Conclusions. Light nuclei should be systematically considered in the analysis of transport parameters. They bring independent constraints which are competitive with those obtained from the B/C analysis.

Key words. Astroparticle physics – Methods: statistical – ISM: cosmic rays

1. Introduction

Secondary species in Galactic cosmic rays (GCRs) are produced during the CR journey from the acceleration sites to the solar neighbourhood, by means of nuclear interactions of heavier primary species with the interstellar medium. Hence, they are tracers of the CR transport in the Galaxy (e.g., Strong et al. 2007). Studying secondary-to-primary ratios is useful as it factors out the 'unknown' source spectrum of the progenitor, leaving ^{2}H/^{4}He, ^{3}He/^{4}He, B/C, sub-Fe/Fe—and recently $\bar{p}/p$ (Putze et al. 2009; di Bernardo et al. 2010)—suitable quantities to constrain the transport parameters for species $Z \leq 30$.

Most secondary-to-primary ratios have $A/Z \sim 2$, and in that respect, ^{3}He/^{4}He is unique since it probes a different regime and allows to address the issue of the 'universality' of propagation histories. For instance, in an analysis in the leaky-box model (LBM) framework, Webber (1997) found that ^{3}He/^{4}He data imply a similar propagation history for the light and heavier species (which was disputed in earlier papers). Webber also argued that the situation with regard to the ^{2}H/^{4}He ratio is less clear, because the uncertainties on the measurements are large (mainly due to instrumental and atmospheric corrections). H and He spectra are the most abundant species in the cosmic radiation, and thus ^{2}H and ^{3}He are the most abundant secondary species in GCRs. However, achieving a good mass resolution—especially at high energy—is experimentally challenging. This explains why the elemental B/C ratio received more focus both experimentally and theoretically (thanks to its higher precision data w.r.t. to the quartet data).

From the modelling side, after the first thorough and pioneering studies performed in the 60's-70's (Badhwar & Daniel 1963; Ramaty & Lingenfelter 1969; Meyer 1972; Mitler 1972; Ramadurai & Biswas 1974; Mewaldt et al. 1976), the interest for the quartet nuclei somewhat stalled. Several updated analyses of the propagation parameters from the quartet were published as new data became available (see Table A.1 for references). However, very few dedicated studies were carried out in the 80's (Beatty 1986; Webber et al. 1987), likewise in the 90's (Webber 1990a; Seo & Ptuskin 1994; Webber 1997), and none in the 00's. This is certainly related to the very slow pace at which new data became available in this period. Curiously, the most recent published data have not really been properly interpreted, i.e. for ^{2}H/^{4}He data, IMAX92 (de Nolfo et al. 2000) and AMS-01 (Aguilar et al. 2011); and for ^{3}He/^{4}He data, IMAX92 (Menn et al. 2000), SMILI-II (Ahlen et al. 2000), AMS-01 (Xiong et al. 2003), BESS98 (Myers et al. 2003), CAPRICE98 (Mocchiutti et al. 2003). Furthermore, almost all analyses have been performed in

Send offprint requests to: B. Coste, coste@lpsc.in2p3.fr

the successful but simplistic LBM, but in a few studies[1]. At the same time, the analysis of the B/C ratio has been scrutinised in more details. For instance, to replace the old usage of matching the data by means of an inefficient manual scan of the parameter space (e.g., Jones et al. 2001), more systematic scans were carried out (on the B/C and sub-Fe/Fe ratio) to get best-fit values as well as uncertainties on the parameters (Maurin et al. 2001; Lionetto et al. 2005; Evoli et al. 2008; di Bernardo et al. 2010). A recent improvement is the use of Markov Chain Monte Carlo (MCMC) techniques to directly access the probability-density function (PDF) of the GCR transport and source parameters (Putze et al. 2009, 2010, 2011; Trotta et al. 2011).

In this paper, we revisit the constraints set by the quartet nuclei and their consistency with the results of heavier nuclei. In the context of the forthcoming PAMELA and AMS-02 data on these ratios, we also discuss the strategy to adopt and intrinsic limitations of the transport parameters reconstruction. For that purpose, we take advantage of the data taken in the last decade as well as simulated data of any precision, and analyse them with an MCMC technique implemented in the USINE propagation code. This extends and complements analyses of the B/C and primary nuclei (Putze et al. 2010, 2011) in a 1D diffusion model.

The paper is organised as follows. In Sect. 2, we briefly recall the main ingredients of the 1D diffusion model and the MCMC analysis. We also list the parameters which are constrained. The simulated data and their analysis are described in Sect. 3. The analysis of the real data is given in Sect. 4. We conclude in Sect. 5. Appendix A gathers the data sets and the updated cross-sections used in the quartet analysis.

2. MCMC technique, propagation and parameters

The MCMC technique and its use in the USINE propagation code is detailed in Putze et al. (2009) and summarised in Putze et al. (2010). The full details regarding the 1D transport model can be found in Putze et al. (2010). Below, we only provide a brief description.

2.1. An MCMC technique for the PDF of the parameters

The MCMC method, based on Bayesian statistics, is used to estimate the full distribution (conditional PDF) given some experimental data and some prior density for these parameters. Our chains are based on the Metropolis-Hastings algorithm, which ensures that the distribution of the chain asymptotically tends to the target PDF.

The chain analysis refers to the selection of a subset of points from the chains (to get a reliable estimate of the PDF). The steps at the beginning of the chain are discarded (burn-in length) if they are too far of the region of interest. Sets of independent samples are obtained by thinning the chain (over the correlation length). The final results of the MCMC analysis are the joint and marginalised PDFs. They are obtained by counting the number of samples within the related region of the parameter space.

[1] Seo & Ptuskin (1994) used a 1D diffusion model with reacceleration whereas Webber & Rockstroh (1997) relied on a Monte Carlo calculation; both studies conclude similarly (consistency with the grammage required for heavier species to produce the light secondaries). A preliminary effort based on the GALPROP propagation code was also carried out in Moskalenko et al. (2003).

2.2. 1D Propagation model and parameters

The Galaxy is modelled to be an infinite thin disc of half-thickness h, which contains the gas and the sources of CRs. The diffusive halo region (where the gas density is assumed to be equal to 0) extends to $+L$ and $-L$ above and below the disc. A constant wind $\boldsymbol{V}(\boldsymbol{r}) = \mathrm{sign}(z) \cdot V_c \times \boldsymbol{e}_z$, perpendicular to the Galactic plane, is assumed. In this framework, CRs diffuse in the disc and in the halo independently of their position. Such semi-analytical models are faster than full numerical codes (GALPROP[2] and DRAGON[3]), which is an advantage for sampling techniques like MCMC approaches.

2.2.1. Transport equation

The differential density N^j of the nucleus j is a function of the total energy E and the position $\boldsymbol{r}$ in the Galaxy. Assuming a steady state, the transport equation can be written in a compact form as

$$\mathcal{L}^j N^j + \frac{\partial}{\partial E}\left(b^j N^j - c^j \frac{\partial N^j}{\partial E}\right) = \mathcal{S}^j \ . \tag{1}$$

The operator $\mathcal{L}$ (we omit the superscript j) describes the diffusion $K(\boldsymbol{r}, E)$ and the convection $\boldsymbol{V}(\boldsymbol{r})$ in the Galaxy, but also the decay rate $\Gamma_{\rm rad}(E) = 1/(\gamma\tau_0)$ if the nucleus is radioactive, and the destruction rate $\Gamma_{\rm inel}(\boldsymbol{r}, E) = \sum_{ISM} n_{\rm ISM}(\boldsymbol{r}) v \sigma_{\rm inel}(E)$ for collisions with the interstellar matter (ISM), in the form

$$\mathcal{L}(\boldsymbol{r}, E) = -\boldsymbol{\nabla} \cdot (K \boldsymbol{\nabla}) + \boldsymbol{\nabla} \cdot \boldsymbol{V} + \Gamma_{\rm rad} + \Gamma_{\rm inel}. \tag{2}$$

The coefficients b and c in Eq. (1) are respectively first and second order gains/losses in energy, with

$$b\,(\boldsymbol{r}, E) \ = \ \langle \frac{dE}{dt} \rangle_{\rm ion,\,coul.} - \frac{\boldsymbol{\nabla}.\boldsymbol{V}}{3} E_k \left(\frac{2m + E_k}{m + E_k}\right) + \ \frac{(1+\beta^2)}{E} \times K_{\rm pp}, \tag{3}$$

$$c\,(\boldsymbol{r}, E) \ = \ \beta^2 \times K_{\rm pp}. \tag{4}$$

In Eq. (3), the ionisation and Coulomb energy losses are taken from Mannheim & Schlickeiser (1994) and Strong & Moskalenko (1998). The divergence of the Galactic wind $\boldsymbol{V}$ gives rise to an energy loss term related to the adiabatic expansion of cosmic rays. The last term is a first order contribution in energy from reacceleration. Equation (4) corresponds to a diffusion in momentum space, leading to an energy gain. The associated diffusion coefficient $K_{\rm pp}$ (in momentum space) is taken from the model of minimal reacceleration by the interstellar turbulence (Osborne & Ptuskin 1988; Seo & Ptuskin 1994). It is related to the spatial diffusion coefficient K by

$$K_{\rm pp} \times K = \frac{4}{3} V_a^2 \ \frac{p^2}{\delta\,(4-\delta^2)\,(4-\delta)}, \tag{5}$$

where V_a is the Alfvénic speed in the medium.

We refer the reader to App. A of Putze et al. (2010) for the solution to Eq. (1) in the 1D geometry.

[2] http://galprop.stanford.edu/

[3] http://www.desy.de/~maccione/DRAGON/

Table 1. Models tested in the paper.

Model	Transport parameters	Description
II	$\{K_0, \delta, V_a\}$	Diffusion + reacceleration
III	$\{K_0, \delta, V_c, V_a\}$	Diff. + conv. + reac.

Note 1. For the sake of consistency, the model identification follows that of Putze et al. (2009, 2010, 2011) and Maurin et al. (2010).

2.2.2. Free parameters of the analysis

The exact energy dependence of the source and transport parameters is unknown, but they are expected to be power laws of $\mathcal{R} = pc/Ze$ (rigidity of the particle).

The low-energy diffusion coefficient requires a $\beta = v/c$ factor that takes into account the inevitable effect of particle velocity on the diffusion rate. However, the recent analysis of the turbulence dissipation effects on the transport coefficient has shown that this coefficient could increase at low-energy (Ptuskin et al. 2006; Shalchi & Büsching 2010). Following Maurin et al. (2010), it is parametrised to be

$$K(E) = \beta^{\eta_T} \cdot K_0 \mathcal{R}^{\delta} \ . \tag{6}$$

The default value used for this analysis is $\eta_T = 1$. The two other transport parameters are V_c, the constant convective wind perpendicular to the disc, and V_a, the Alfvénic speed regulating the reacceleration strength [see Eq. (5)]. The two models considered in this paper are given in Table 1.

The low-energy primary source spectrum from acceleration models (e.g., Drury 1983; Jones 1994) is also unknown. We parametrise it to be

$$Q_{E_{k/n}}(E) \equiv \frac{dQ}{dE_{k/n}} = q \cdot \beta^{\eta_S} \cdot \mathcal{R}^{-\alpha}, \tag{7}$$

where q is the normalisation. The reference low-energy shape corresponds to $\eta_S = -1$ (to have $dQ/dp \propto p^{-\alpha}$, i.e. a pure power-law).

The halo size of the Galaxy L cannot be solely determined from secondary-to-primary stable ratios and requires a radioactive species to lift the degeneracy between K_0 and L. However, the range of allowed values is still very loosely constrained (e.g., Putze et al. 2010). As the transport and source parameters can always be rescaled would a different choice of L assumed (see the scaling relations given in Maurin et al. 2010, where δ is shown not to depend on L), we fix it to $L = 4$ kpc. This will also ease the comparison of the results obtained in this paper with those of our previous studies (Putze et al. 2010, 2011).

3. MCMC analysis on artificial data sets

MCMC techniques make the scan of high-dimensional parameter spaces possible, such that a simultaneously estimation of transport and source parameters is possible (Putze et al. 2009). However, transport parameters are shown to be strongly degenerated for the B/C ratio data in the range $0.1 - 100$ GeV/nuc (Maurin et al. 2010), and source and transport parameters are correlated (Putze et al. 2009, 2010). For GCR data in general, the fact that primary fluxes and secondary fluxes are not measured to the same accuracy[4] can bias or prevent an accurate determination of these parameters: a simultaneous fit has been observed to be driven by the more accurately measured primary flux (Putze et al. 2011). This, although statistically correct, might not maximise the information obtained on the transport parameters. Therefore, several strategies can be considered when dealing with GCR data:

- a combined analysis of secondary-to-primary ratio and primary flux to constrain simultaneously the source and transport parameters;
- a secondary-to-primary ratio analysis only, either fixing the source parameters (i.e., using a strong prior), or using a loose prior.
- a primary flux analysis only, either fixing the transport parameters (i.e., using a strong prior), or using a loose prior.

In the literature, the strong prior approach has almost always been used to determine the transport or the source parameters. The issue we wish to address is how sensitive the sought parameters are to various strategies. This is the motivation to introduce artificial data, i.e. an ideal case study, as opposed to the case of real data where several other complications can arise (systematics in the data and/or the use of the incorrect propagation model or solar modulation model/level).

3.1. Sets of artificial data

To be as realistic as possible, we choose models that roughly reproduce the actual data points (see Fig. 4), but also match the typical energy coverage, number of data points, central value and spread (error bars) of the measurements[5]. To speed-up the calculation and for this section only, we assume that all ^{3}He comes from ^{4}He (see Sect. 4.1 for all the relevant progenitors). No systematic errors were added although they may set a fundamental limitation in recovering the cosmic-ray parameters. In practice, the statistical errors for the artificial data sets correspond to the sigma of the standard Gaussian deviations used to randomise the data points around their model value: ^{3}He/^{4}He was generated with statistical errors of 10% while He fluxes were generated with 1% and 10% errors, to simulate the situation where primary fluxes are 'more accurately' or 'equally' measured (in terms of statistics) than the secondary-to-primary ratio.

The parameters of the two models used to simulate the data are listed in the two *italic* lines in Table 2, denoted *Model II* and *Model III*. They correspond to extreme values of the diffusion slope δ, but which still roughly fall in the range of values found for instance from the B/C analysis (Putze et al. 2010): for *Model II* with reacceleration only ($V_c = 0$), δ is generally found to fall between 0.1 and 0.3, whereas for *Model III* with convection and reacceleration, δ is generally found to fall into the $0.6-0.8$ range (Jones et al. 2001; Maurin et al. 2010).

[4] Statistical uncertainties are smaller for primary fluxes (more abundant than secondary fluxes), but the latter a more prone to systematics than ratios (e.g. secondary-to-primary ratios used to fit transport parameters).

[5] The uncertainty on the H and He fluxes is a few percents (for the recent PAMELA data, Adriani et al. 2011) and several tens of percents for the ^{3}He/^{4}He ratio.

Table 2. Simulated data analysis for several *Models* (input parameters in *italic*) with $L = 4$ kpc: each line corresponds to the MCMC-reconstructed values (most-probable value, and relative uncertainties corresponding to the 68% CI) based on a given data/parameters option (see Sect. 3.2). The last column gives the value of the best χ^2/d.o.f. configuration found (corresponding to the curves shown in Fig. 1).

Option: data/params	η_T -	$K_0 \times 10^2$ (kpc^2 Myr^{-1})	δ -	V_c (km s^{-1})	V_a (km s^{-1})	α -	η_S -	$\chi^2_{\rm best}$/d.o.f. -
				Model II				
	1	*10.0*	*0.2*	...	*70*	*2.3*	*1*	...
1: ^{3}He/^{4}He+He$^{10\%}$	[1]	$10.3^{+3.9\%}_{-3.9\%}$	$0.185^{+54\%}_{-5.4\%}$	...	$72.7^{+6.3\%}_{-5.6\%}$	$2.29^{+0.9\%}_{-1.3\%}$	$0.78^{+13.\%}_{-17.\%}$	0.93
2: ^{3}He/^{4}He+He$^{1\%}$	[1]	$10.2^{+2.0\%}_{-3.9\%}$	$0.192^{+3.1\%}_{-2.1\%}$	...	$73.0^{+2.7\%}_{-4.1\%}$	$2.29^{+0.3\%}_{-0.3\%}$	$0.88^{+3.4\%}_{-5.7\%}$	1.08
2': 2 + src=true	[1]	$9.7^{+3.1\%}_{-3.1\%}$	$0.199^{+3.0\%}_{-4.0\%}$	...	$68.0^{+4.4\%}_{-2.9\%}$	[2.3]	[1]	0.97
3: ^{3}He/^{4}He	[1]	$11.5^{+13.\%}_{-23.\%}$	$0.19^{+21\%}_{-16\%}$	...	$39.4^{+68.\%}_{-53.\%}$	$2.70^{+148\%}_{-85\%}$	$1.5^{+326\%}_{-106\%}$	0.87
3': 3 + src=true	[1]	$10.1^{+3.0\%}_{-4.0\%}$	$0.196^{+5.1\%}_{-7.1\%}$	...	$69.6^{+5.9\%}_{-6.6\%}$	[2.3]	[1]	0.88
4: ^{3}He/^{4}He + src=prior	[1]	$9.0^{+11.\%}_{-11.\%}$	$0.2^{+15.\%}_{-10.\%}$	...	$73.3^{+5.5\%}_{-8.2\%}$	[1.8, 2.5]	$[-2, +2]$	1.08
				Model III				
	1.5	*0.75*	*0.7*	*18*	*41*	*2.3*	*1*	...
1: ^{3}He/^{4}He+He$^{10\%}$	$1.66^{+42.\%}_{-13.\%}$	$1.5^{+40.\%}_{-47.\%}$	$0.51^{+33.\%}_{-7.8\%}$	$18.4^{+17.\%}_{-10.\%}$	$54.1^{+18.\%}_{-8.9\%}$	$2.29^{+0.9\%}_{-1.7\%}$	$1.^{+7.0\%}_{-36.\%}$	1.43
2: ^{3}He/^{4}He+He$^{1\%}$	$1.42^{+2.8\%}_{-1.4\%}$	$0.62^{+9.7\%}_{-9.7\%}$	$0.725^{+0.8\%}_{-3.7\%}$	$19.7^{+3.6\%}_{-4.1\%}$	$37.1^{+9.2\%}_{-1.3\%}$	$2.334^{+0.3\%}_{-1.1\%}$	$0.98^{+4.1\%}_{-2.0\%}$	1.00
2': 2 + src=true	$1.48^{+0.7\%}_{-0.7\%}$	$0.7^{+4.3\%}_{-5.7\%}$	$0.71^{+1.4\%}_{-1.4\%}$	$18.3^{+1.6\%}_{-3.3\%}$	$40.7^{+2.7\%}_{-2.2\%}$	[2.3]	[1]	1.01
3: ^{3}He/^{4}He	$1.47^{+8.8\%}_{-12.\%}$	$0.92^{+89.\%}_{-48.\%}$	$0.57^{+21.\%}_{-14.\%}$	$20.5^{+18.\%}_{-14.\%}$	$58.0^{+22.\%}_{-15.\%}$	$0.12^{+708\%}_{-92.\%}$	$-2.2^{+50.\%}_{-36.\%}$	0.83
3': 3 + src=true	$1.34^{+29.\%}_{-0.7\%}$	$0.48^{+139\%}_{-60.\%}$	$0.68^{+24.\%}_{-22.\%}$	$18.1^{+6.1\%}_{-3.3\%}$	$44.8^{+14.\%}_{-28.\%}$	[2.3]	[1]	0.89
4: ^{3}He/^{4}He + src=prior	$1.38^{+13.\%}_{-16.\%}$	$0.37^{+132\%}_{-62.\%}$	$0.65^{+29.\%}_{-1.7\%}$	$20.3^{+13.\%}_{-4.0\%}$	$42.2^{+15.\%}_{-25.\%}$	[1.8, 2.5]	$[-2, +2]$	0.96
				Model III: analysis with Model II				
	1.5	*0.75*	*0.7*	*18*	*41*	*2.3*	*1*	...
1: ^{3}He/^{4}He+He$^{10\%}$	[1]	$13.8^{+3.6\%}_{-5.1\%}$	$0.21^{+4.8\%}_{-4.8\%}$	...	$126^{+4.8\%}_{-4.0\%}$	$2.3^{+0.9\%}_{-1.7\%}$	$0.24^{+42.\%}_{-29.\%}$	4.0
2: ^{3}He/^{4}He+He$^{1\%}$	[1]	$11.4^{+3.5\%}_{-1.8\%}$	$0.263^{+3.8\%}_{-3.8\%}$	...	$85^{+2.4\%}_{-3.5\%}$	$2.4^{+0.4\%}_{-0.4\%}$	$1.19^{+1.7\%}_{-3.4\%}$	18
4: ^{3}He/^{4}He + src=prior	[1]	$20.7^{+20.\%}_{-8.2\%}$	$0.089^{+31.\%}_{-18.\%}$	...	$107^{+5.6\%}_{-12.\%}$	[1.8, 2.5]	$[-2, +2]$	2.1
				Model II: analysis with Model III				
	1	*10.0*	*0.2*	*0*	*70*	*2.3*	*1*	...
1: ^{3}He/^{4}He+He$^{10\%}$	$1.37^{+5.1\%}_{-4.4\%}$	$4.0^{+65\%}_{-45\%}$	$0.29^{+24\%}_{-21\%}$	$17.2^{+9.3\%}_{-41\%}$	$73.5^{+7.2\%}_{-17\%}$	$2.21^{+1.8\%}_{-0.5\%}$	$0.80^{+12\%}_{-29\%}$	0.97
2: ^{3}He/^{4}He+He$^{1\%}$	$0.87^{+9.2\%}_{-5.7\%}$	$7.4^{+19\%}_{-27\%}$	$0.25^{+20\%}_{-8.0\%}$	$8.6^{+62\%}_{-50\%}$	$76.3^{+3.5\%}_{-4.8\%}$	$2.23^{+0.4\%}_{-0.4\%}$	$0.68^{+7.4\%}_{-10\%}$	1.1
4: ^{3}He/^{4}He + src=prior	$0.43^{+193\%}_{-107\%}$	$4.9^{+49\%}_{-73\%}$	$0.24^{+50\%}_{-21\%}$	$18.4^{+12\%}_{-59\%}$	$69.9^{+12\%}_{-18\%}$	[1.8, 2.5]	$[-2, +2]$	1.05

Note 2. A value in square brackets corresponds to the fixed value of the parameter for the analysis. An interval in square brackets corresponds to the prior used for the analysis (the posterior PDF obtained is close to the prior).

3.2. Strategies to analyse the data

To test the impact on the reconstruction of the *transport* (η_T, K_0, δ, V_a, and V_c) and/or *source* (α and η_S) parameters, we test the following combinations (data set|model parameters) for the analysis.

^{3}He/^{4}He + He data

Option 1 ($\sigma_{\rm He}=10\%$): *transport* + *source*;
Option 2 ($\sigma_{\rm He}=1\%$): *transport* + *source*;
Option 2' ($\sigma_{\rm He}=1\%$): *transport* (source = 'true' value);

^{3}He/^{4}He ratio only

Option 3: *transport* + *source*;
Option 3': *transport* (source = 'true' value);
Option 4: *transport* (source = weak prior).

We find that the He data alone cannot constrain the transport parameters (not shown here), in agreement with Putze et al. (2011) results (strong degeneracy between α and δ, but also with K_0, V_a, and η_T).

3.3. Analysis of the artificial data

In a first step, we used the MCMC technique to estimate the best-fit parameters. The ^{3}He/^{4}He ratio and ^{4}He flux are shown for model II (crosses) and the corresponding simulated data (plusses) in Fig. 1. When both the ^{3}He/^{4}He and ^{4}He data are included in the fit (options 1 and 2, red dotted and red solid lines), the initial flux (crosses) is perfectly recovered for ^{4}He, and very well recovered for ^{3}He/^{4}He. When the fit is only based on ^{3}He/^{4}He (options 3 and 5, magenta

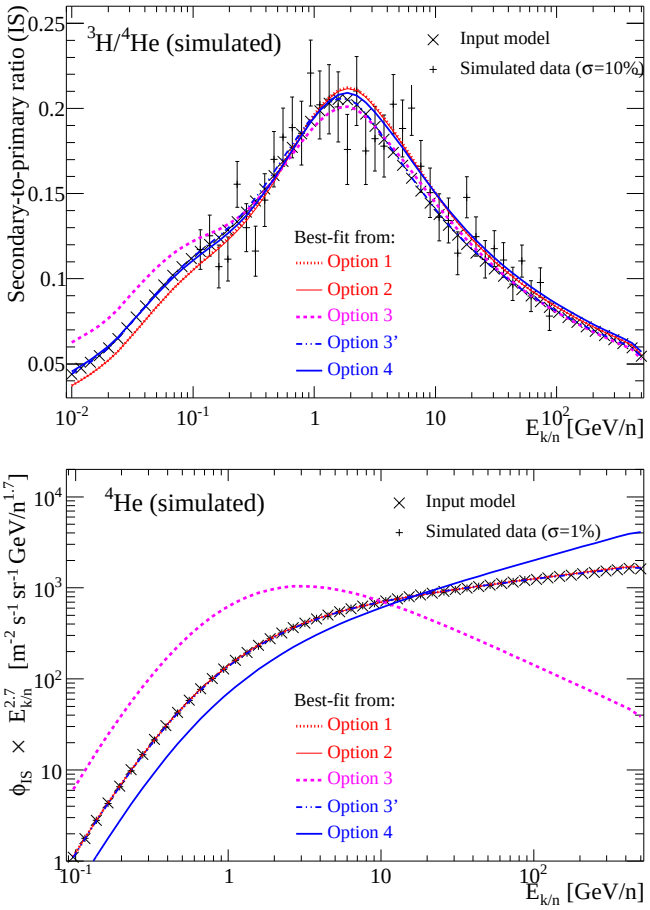


Fig. 1. Analysis of simulated interstellar (IS) data sets for the ^{3}He/^{4}He ratio (top panel) and the ^{4}He flux times $E_{k/n}^{2.7}$ (bottom panel) based on Model II (× symbols), the parameters of which are given in Table 2). The best-fit reconstructed curves correspond to the different 'options' given in Sect. 3.2.

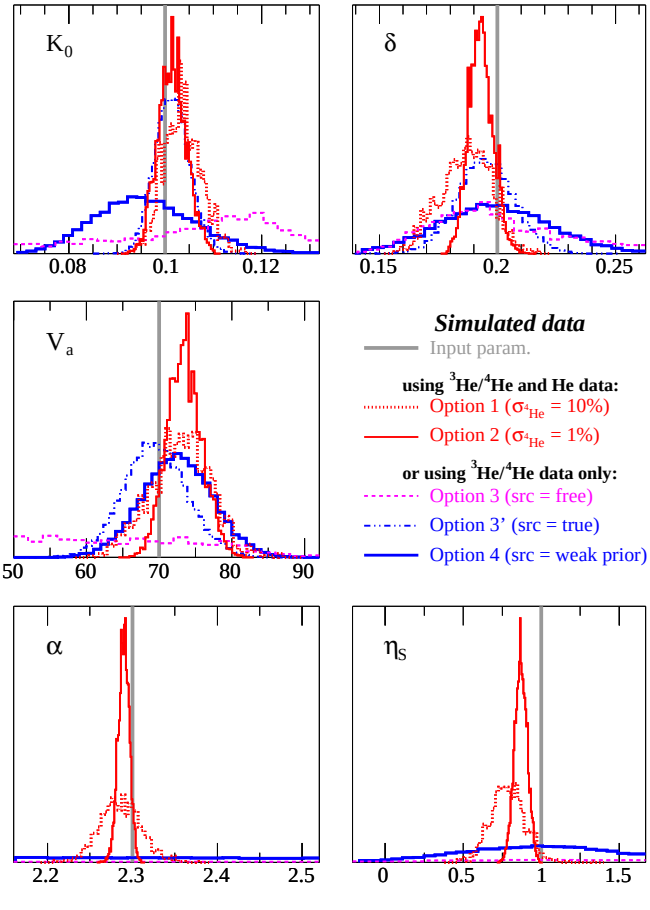


Fig. 2. Marginalised posterior PDF for the transport and source parameters on the artificial data for Model II (the values for the input model are shown as thick vertical grey lines in each panel). The colour code and style correspond to the five 'options' described in Sect. 3.2 (and used in Fig. 1).

dashed and blue solid lines), the initial flux is obviously not recovered (unless the source parameters are set to the true value as in option 3'), but the ^{3}He/^{4}He ratio is consistent with the data. Unsurprisingly, the associated $\chi^2_{\rm best}$/d.o.f. values (last column of Table 2) are close to 1.

The MCMC analysis allows us to go further as it provides the PDF of the parameters, from which the most-probable value and confidence intervals (CIs) are obtained. The results are gathered in Table 2 and Fig. 2. The various panels of the latter represent the PDFs for transport and source parameters for each 'option' for Model II. (For concision the correlation plots are not shown.) From these plots, some arguments are in favour of a simultaneous use of the secondary-to-primary ratio and the primary flux (here, ^{3}He/^{4}He and He), but not all.

3.3.1. Advantages from a simultaneous analysis (ratio + flux)

A simultaneous analysis (^{3}He/^{4}He + He) gives more stringent constraints on the transport parameters than only analysing the secondary-to-primary ratio (compare the PDFs for the red curves and blue curves in Fig. 2 respectively, for K_0, δ, and V_c). This partly comes from the observed correlations between transport and source parameters[6] (e.g., Putze et al. 2009). Option 2' and option 3' with fixed source parameters show that the better CIs on the transport parameters come from the information contained in primary fluxes[7]. The same conclusions hold true for Model III ($V_c \neq 0$), although with larger relative uncertainties due to the two extra transport parameters of the model (η_T and V_c).

3.3.2. What if the wrong model is used?

As an illustration, we analyse data simulated from model III ($V_c \neq 0$) with model II ($V_c = 0$) and vice versa (lower half of Table 2). If we force $V_c = 0$ (while $V_c^{\rm true} = 18$ km s^{-1}), the diffusion slope goes to a low value $\delta \sim 0.2$ ($\delta^{\rm true} = 0.7$), while the Alfvénic speed goes to a high value $V_a \sim 100$ km s^{-1} ($V_a^{\rm true} = 41$ km s^{-1}). The larger

[6] More stringent constraints on the source parameters (from more precise data) leads to more stringent constraints on the transport values: option 1 ($\sigma_{\rm He}$=10%) vs option 2 ($\sigma_{\rm He}$=1%).

[7] Note that the lack of constraints on the source parameters for option 4 confirms that the secondary-to-primary ratio is only marginally sensitive to the source parameters (e.g., Putze et al. 2011).

$\chi^2_{\rm best}$/d.o.f. value with respect to the one obtained fitting the correct model easily disfavours this model. The second test (simulated with II, analysed with III) indicates whether allowing for more freedom in the analysis (two additional free parameters η_T and V_c) affects the recovery of the parameters. The values of $\delta^{\rm true} = 0.2$ and $V_a^{\rm true} = 70$ km s^{-1} are recovered, while the others are systematically offset but less than 3σ away from their true value. In this simple example, adding extra parameters is not an issue as the $\chi^2_{\rm best}$/d.o.f. still favours the minimal model. However, with real data (see Sect. 4.3 and the B/C analysis of Putze et al. 2010; Maurin et al. 2010), in such a situation, it is so far impossible to conclude whether the correct model is used, due to the possible issue of multimodality and biases from systematics (see below).

3.3.3. Drawbacks from a simultaneous analysis

For Model II but even more for Model III (which has more free transport parameters), a possible worry is the presence of multimodal PDF distributions, which more often happens for the simultaneous analysis. An example of multimodality is the analysis with Model II (i.e. $V_a = 0$) of data simulated with Model III, which corresponds to a local minimum of the true Model III parameters. This is of no consequence for the ideal case, but real data may suffer from systematics errors and/or the inappropriate solar modulation model may be chosen. In that case, the true minimum can be displaced, or turned into a local minimum (and vice versa). Measurements over the last decades showed that primary fluxes are more prone to systematics than secondary-to-primary ratios. Primary fluxes are also more sensitive to solar modulation than ratios. For these reasons, the use of secondary-to-primary data only (option 4) for the analysis, although less performant to get stringent limits on the transport parameters, is expected to be more reliable and robust.

3.4. Recommended strategy to analyse real data

The most robust approach to determine the transport parameters (and their CIs) is to analyse the secondary-to-primary ratio using a loose but physically-motivated prior on the source parameters (option 4). This has the advantage of taking into account the correlations between the source and transport parameters. The simultaneous analysis is mandatory to obtain the source parameters (option 1 or 2). It also brings more information on the transport parameters, but the primary fluxes can bias their determination if it suffers from systematics. We recommend such an analysis to be performed in addition to the direct secondary-to-primary ratio analysis, in order to get the following diagnosis: if the range of values for the transport parameters from both analyses are

- *inconsistent*, it indicates that the values and CIs obtained for the sources parameters are biased or unreliable;
- *consistent*, the selected propagation model may be the correct one, and the source parameters are then the most probable ones for this model. However, the CIs on the transport parameters are very likely to be underestimated if the error bars on the ratio are much larger than the ones on the primary fluxes.

Obviously, our analysis does not cover the range of all systematics when dealing with real data. A more systematic analysis—e.g. covering a wider family of propagation models, several solar modulation models, several sources of systematics in the data— goes far beyond the scope of this paper. Note that some of these effects are likely to be energy dependent, complicating even further the analysis. With the successful installation of the AMS-02 detector on the ISS and its expected high-precision data, these issues are bound to gain importance.

4. Constraints from the quartet data

We now apply the MCMC technique to the analysis of real data. We emphasise that for the artificial ones, we assumed the ^{3}He to come solely from the ^{4}He fragmentation, in order to speed up the calculation. Based on our new compilation for the cross-section formulae (see App. B), we take into account the contributions from $A > 4$ CR parents, checking which parents are relevant (§4.1). Having determined the heaviest parent to consider in the calculation, we then move on to the result of the MCMC analysis (§4.2), and those from our best analysis (§4.3).

4.1. Fractional contributions

At first order, the contribution to the ^{2}H and ^{3}He secondary production from $Z > 4$ nuclei is proportional to the source term $\mathcal{S}^j$ [see Eq. (1)]. For a secondary contribution, the source term is proportional to the primary flux of the parents (which have been measured by many experiments), and to the production cross-section. Normalised to the production from ^{4}He, we have

$$\mathrm{Rel}^{\rm P\to S} \propto \frac{\mathcal{S}^{\rm P}}{\mathcal{S}^{\rm He}} \propto \frac{\Phi_{\rm P}}{\Phi_{^4{\rm He}}} \cdot \gamma_P^{\rm S}, \tag{8}$$

where P is the CR projectile, S is the secondary fragment considered, and $\gamma_{\rm P}^{\rm S}$ [see Eq. (B.3)] is the production cross-section relative to the production from ^{4}He. The fractional contribution $f^{\rm P\to S}$ for each parent is defined to be

$$f^{\rm P\to S} = \frac{\mathrm{Rel}^{\rm P\to S}}{\sum_{\rm P'={He\cdots Ni}} \mathrm{Rel}^{\rm P'\to S}}. \tag{9}$$

As seen from Table 3, the most important contributions from primary species heavier than He ($Z > 2$) are C and O, followed by Mg and Si and finally Fe. The total contribution of these species amounts to $\sim 35\%$ for ^{2}H and $\sim 11\%$ for ^{3}He, but mixed species (such as N) or less abundant species also contribute to $\sim 5\%$.

A proper calculation of these fractional contributions involves the full solution of the propagation equation, taking into account energy gains and losses, total inelastic reactions, and convection. Based on the propagation parameters found to fit best the current data (see next section), we show in Fig. 3 the fractional contribution of $A > 4$ nuclei as a function of energy for the full calculation. It confirms the previous figures, but with a residual energy dependence (itself depending on the species) hitting a plateau above $\sim$ 100 GeV/n. The difference can be mostly attributed to a preferential destruction of heavier nuclei at

Table 3. Estimated fractional contribution of projectile $A > 4$ to the ^{2}H and ^{3}He fluxes. The columns are respectively the name of the element, atomic number, ratio of measured fluxes, production cross-section ratios for ^{2}H and ^{3}He, and the estimated fractional contribution to ^{2}H and ^{3}He.

P	A_P	$\frac{\Phi_P}{\Phi_{^4He}}$	$\gamma_P^{^2H}$	$\gamma_P^{^3He}$	$f^{P\to^2H}$ %	$f^{P\to^3He}$ %
He	4	1.0	···	···	60.1	86.0
C	12	$3.3\,10^{-2}$	5.5	2.3	7.5	3.6
N	14	$7.4\,10^{-3}$	6.6	2.4	2.0	0.8
O	16	$3.4\,10^{-2}$	7.8	2.6	10.7	4.1
F	19	$5.2\,10^{-4}$	9.6	2.8	0.2	0.1
Ne	22	$5.1\,10^{-3}$	11.4	3.1	2.4	0.8
Na	23	$8.8\,10^{-4}$	12.1	3.2	0.4	0.1
Mg	24	$6.7\,10^{-3}$	12.7	3.3	3.4	1.0
Al	26	$1.1\,10^{-3}$	14.0	3.5	0.6	0.2
Si	28	$5.5\,10^{-3}$	15.3	3.7	3.4	1.0
P	31	$1.8\,10^{-4}$	17.3	4.0	0.1	< 0.1
S	32	$1.0\,10^{-3}$	17.9	4.1	0.7	0.2
Cl	35	$1.8\,10^{-4}$	20.0	4.5	0.1	< 0.1
Ar	36	$3.1\,10^{-4}$	20.6	4.6	0.3	0.1
K	39	$2.1\,10^{-4}$	22.7	5.0	0.2	< 0.1
Ca	40	$6.1\,10^{-4}$	23.4	5.1	0.6	0.1
Sc	45	$1.0\,10^{-4}$	27.0	5.8	0.1	< 0.1
Ti	48	$3.4\,10^{-4}$	29.2	6.2	0.4	0.1
V	51	$1.8\,10^{-4}$	31.4	6.6	0.2	0.1
Cr	52	$3.6\,10^{-4}$	32.1	6.8	0.5	0.1
Mn	55	$3.0\,10^{-4}$	34.3	7.2	0.4	0.1
Fe	56	$3.7\,10^{-3}$	35.1	7.4	5.3	1.3
Ni	58	$2.4\,10^{-4}$	36.6	7.7	0.4	0.1

Note 3. The ratio of measured fluxes is calculated at $\sim$ 10 GeV/n using PAMELA for He (Adriani et al. 2011) and HEAO-3 (Engelmann et al. 1990) for $6 \leq Z \leq 30$.

low energy[8]. Note that for ^{2}H production, the coalescence of two protons (long-dashed pink curve) contributes up to 40% of the total at $\sim$ 1 GeV/n energy (peak of the cross-section, see Fig. B.3). Depending on the precision reached for the data, it is important to include the CNO contribution (e.g. Ramaty & Lingenfelter 1969; Jung et al. 1973b; Beatty 1986), but also all contributions up to Ni.

Finally, the fragmentation of CNO can also affect the ^{1}H and ^{4}He primary fluxes. The peak of contribution occurs at GeV/n as secondary fluxes drop faster than primary fluxes with energy. Fig. 3 shows this contribution to be $\lesssim 10\%$ for ^{4}He. With the high precision measurement from PAMELA and the even better measurements awaited from AMS-02, this will need to be further looked into in the future.

[8] Indeed, the primary-to-primary ratios are not constant. The heavier the nucleus, the larger its destruction cross-section, the more the propagated flux is affected/decreased at low energy, the longer it takes to reach a plateau of maximal contribution at high energy. The observed trend is consistent with the primary-to-primary ratios shown in Fig. 14 of Putze et al. (2011).

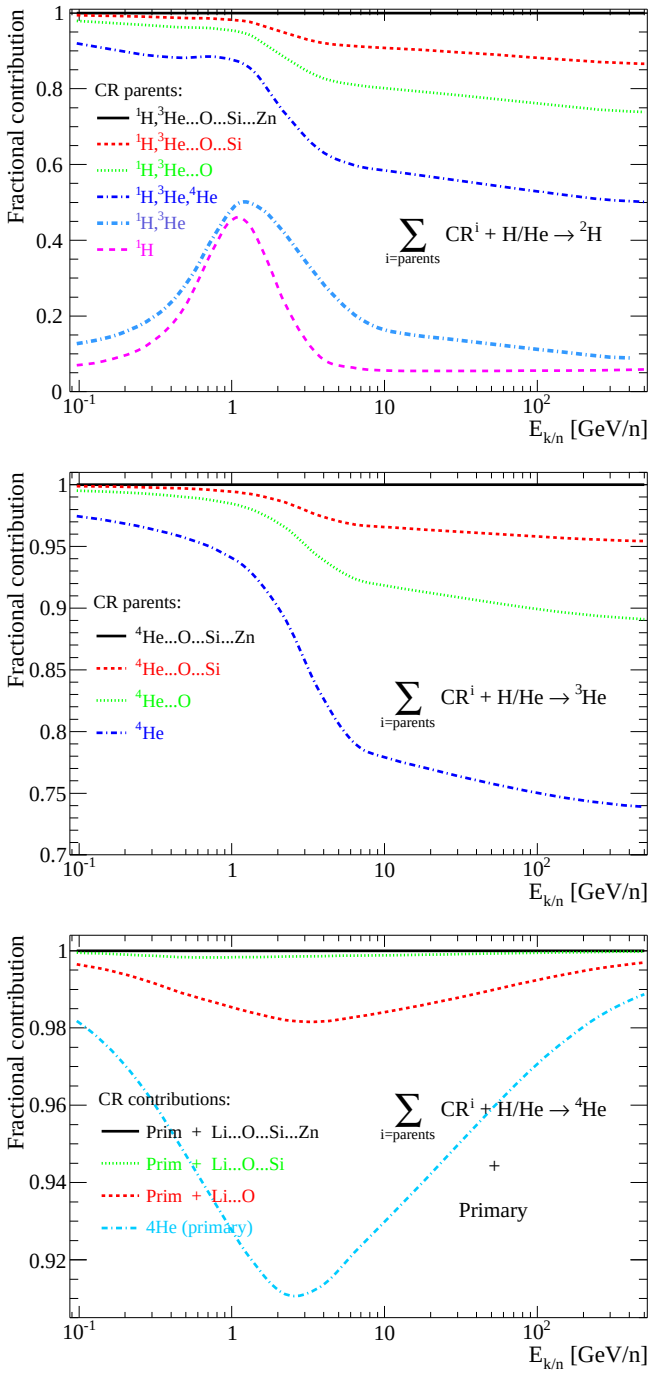


Fig. 3. Fractional contributions to the propagated ^{2}H fluxes (top panel), ^{3}He fluxes (middle panel) and ^{4}He fluxes (bottom panel) as a function of $E_{k/n}$ from $A > 4$ CR parents. For ^{4}He, the primary contribution is also considered.

4.2. MCMC analysis: test of several data combinations

Given the accuracy of current data (see Fig. 4), we must take into account the contribution from all parent nuclei at least up to ^{30}Si. In the rest of the analysis, we use PAMELA data for He (Adriani et al. 2011), as they overcome all others in the $\sim$ GeV−TeV range in terms of precision. Before giving our final results, and to complement Sect. 3.2, we discuss the appropriate choice of data to consider here, in

Table 4. MCMC analysis of Model III ($V_c \neq 0$) with $L = 4$ kpc: most-probable values and relative uncertainties (corresponding to the 68% CI) for the analysis of various combinations of ^{3}He/^{4}He, ^{3}He, and PAMELA He data (+ 3 combinations involving the ^{2}H isotope). The last column gives the χ^2/d.o.f. for the best-fit model found (which usually differs from the most-probable one).

Data	$K_0 \times 10^2$ (kpc^2 Myr^{-1})	δ -	V_c (km s^{-1})	V_a (km s^{-1})	α -	η_S -	$\chi^2_{\rm best}$/d.o.f. -
^{3}He/^{4}He + He	$0.50^{+10\%}_{-12\%}$	$0.79^{+6.4\%}_{-5.2\%}$	$17.3^{+1.7\%}_{-2.5\%}$	$39.5^{+6.1\%}_{-6.6\%}$	$2.26^{+1.8\%}_{-2.7\%}$	$0.07^{+59\%}_{-74\%}$	4.8
^{3}He/^{4}He + He‡	$1.10^{+27\%}_{-27\%}$	$0.54^{+5.6\%}_{-7.4\%}$	$28.0^{+3.6\%}_{-3.6\%}$	$54.0^{+5.6\%}_{-9.3\%}$	$2.49^{+0.4\%}_{-0.8\%}$	$-1.97^{+9.6\%}_{-1.0\%}$	2.1
^{3}He/^{4}He	$0.50^{+84\%}_{-50\%}$	$0.67^{+6.0\%}_{-15\%}$	$27.4^{+3.3\%}_{-4.7\%}$	$41.0^{+34\%}_{-19\%}$	[1.8, 2.5]	[−2, +2]	2.9
^{3}He/^{4}He + ^{3}He	$1.20^{+58\%}_{-8.3\%}$	$0.56^{+11.\%}_{-8.9\%}$	$24.2^{+4.5\%}_{-2.9\%}$	$68.1^{+6.8\%}_{-16.\%}$	$2.23^{+2.7\%}_{-3.6\%}$	$-0.48^{+33\%}_{-52\%}$	1.8
^{3}He/^{4}He + ^{3}He¶	$2.82^{+35\%}_{-50\%}$	$0.39^{+26.\%}_{-5.1\%}$	$24.4^{+6.1\%}_{-8.6\%}$	$85.0^{+7.1\%}_{-22.\%}$	$2.17^{+2.3\%}_{-4.6\%}$	$-0.82^{+18\%}_{-34\%}$	1.9
^{3}He/^{4}He + ^{3}He + He	$0.76^{+10\%}_{-9.2\%}$	$0.79^{+3.8\%}_{-2.5\%}$	$19.6^{+1.4\%}_{-2.8\%}$	$48.1^{+4.0\%}_{-4.8\%}$	$2.22^{+0.9\%}_{-1.8\%}$	$0.02^{+171\%}_{-159\%}$	3.3
^{3}He/^{4}He + ^{3}He¶ + He	$0.81^{+10\%}_{-8.6\%}$	$0.77^{+5.2\%}_{-2.6\%}$	$19.2^{+1.6\%}_{-3.1\%}$	$48.2^{+5.0\%}_{-3.7\%}$	$2.21^{+1.4\%}_{-1.4\%}$	$0.04^{+71\%}_{-63\%}$	3.4
^{2}H/^{4}He + ^{2}H	$15^{+13\%}_{-33\%}$	$0.03^{+100\%}_{-21\%}$	$3.0^{+500\%}_{-67\%}$	$33.7^{+52\%}_{-28\%}$	$2.38^{+4.6\%}_{-3.8\%}$	$-1.15^{+17\%}_{-35\%}$	6.8
^{2}H/^{4}He + ^{2}H + He	$0.53^{+17\%}_{-15\%}$	$0.61^{+8.2\%}_{-6.6\%}$	$14.6^{+3.4\%}_{-2.7\%}$	$26.3^{+8.0\%}_{-11\%}$	$2.47^{+1.2\%}_{-2.4\%}$	$0.47^{+13\%}_{-21\%}$	6.4
^{2}H/^{4}He + ^{2}H + He‡	$6.5^{+55\%}_{-45\%}$	$0.039^{+125\%}_{-125\%}$	$26.1^{+8\%}_{-27\%}$	$24.1^{+39\%}_{-46\%}$	$2.74^{+11\%}_{-11\%}$	$0.38^{+47\%}_{-39\%}$	4.9

¶ Including AMS-01 data from the recently published analysis of Aguilar et al. (2011).
‡ Excluding PAMELA He data points below 5 GeV/n and above 183 GeV/n.

Note 4. An interval in square brackets corresponds to the prior used for the analysis (the posterior PDF obtained is close to the prior).

order to get the best balance between robustness and reliability for the ^{2}H and ^{3}He-related analyses.

4.2.1. Simulated *vs.* real data

We start by comparing the results obtained with the simulated and the actual data set. To avoid lengthy comparisons of numbers, we limit ourselves to Model III (where we also fix η_T to its default value, i.e. 1). The obvious difference with the simulated data is that we no longer have access to the true source parameters (automatically excluding options 2' and 4 discussed in Sect. 3.2). For the simultaneous analysis using He PAMELA data—the precision of which is $\sim 1\%$—, we recover similar values and CIs for the parameters (compare option 2 in Table 2 and the first three lines of Table 4). The second row of Table 4 is based on a subset of He data: high energy data points are discarded because they show departure from a single power-law (Ahn et al. 2010; Adriani et al. 2011), whereas low-energy data points are discarded because of their sensitivity to solar modulation, which is presumably too crudely described by the Force-Field approximation used here. The $\chi^2_{\rm best}$/d.o.f. value (first row) shows that the model has difficulty to perfectly match the high precision PAMELA He data over the whole energy range. The analysis of ^{3}He/^{4}He ratio using a prior on the source parameters (option 4 in Table 2 and third line of Table 4) gives larger CIs for the transport parameters. The consistency between the results of the latter analysis (third line) and that based on the partial He data (second line), and their discrepancy with the results of the analysis based on the full He data set (first line) confirms our suspicion that high precision measurements for primary fluxes can bias the transport parameters determination.

4.2.2. Adding the secondary ^{3}He flux in the analysis

Replacing He by ^{3}He in the simultaneous analysis (4$^{\rm th}$ and 5$^{\rm th}$ line) further affects the determination of the transport parameters. This is not surprising since ^{3}He data are not all consistent with one another (see Fig. 4). The bias is stronger when taking into account the recently published AMS-01 data (Aguilar et al. 2011). If both ^{3}He and He are taken into account[9], the much better accuracy of the He PAMELA data with respect to the ^{3}He data amounts to a smaller weight of the latter in the analysis.

4.2.3. ^{2}H/^{4}He *vs* ^{3}He/^{4}He

We repeat partially the analysis for ^{2}H in the last 3 rows of Table 2. The data are so inconsistent with one another for ^{2}H/^{4}He (see Fig. 4) that we are forced to use at least the ^{2}H flux (whose data points are also markedly inconsistent with one another). Even so, the results are not reliable. PAMELA and AMS-02 have the capability to improve greatly the situation, but in the meantime, we are forced to include He as well in the analysis (next-to-last row in the table). The transport parameter values from the ^{2}H/^{4}He+^{2}H+He analysis are grossly consistent with those from the ^{3}He/^{4}He+^{3}He+He analysis, but are likely to suffer from similar biases (see the previous paragraph). Reducing the energy range of He data is not even possible for the ^{2}H analysis (last line in the table), as the results obtained are not reliable.

[9] The simultaneous analysis of ^{3}He/^{4}He + ^{3}He + He has not been tested in the simulated data since it would have amounted to a double-counting of the ^{3}He data (appearing in the three quantities). However, real data involve different experiments for the various quantities (PAMELA for He and other experiments for ^{3}He), and independent measurements are used.

Table 5. Most-probable values and CIs for Models II and III for our 'best' analysis (Sect. 4.3) of the quartet and B/C data ($L = 4$ kpc).

Data	$K_0 \times 10^2$ (kpc^2 Myr^{-1})	δ -	V_c (km s^{-1})	V_a (km s^{-1})	α -	η_S -	$\chi^2_{\rm best}$/d.o.f. -
Model II							
^{3}He/^{4}He	$15.0^{+0.5}_{-0.5}$	$0.29^{+0.02}_{-0.03}$	-	116^{+11}_{-7}	$[1.8, 2.5]$	$[-2, +2]$	3.3
^{3}He/^{4}He + ^{3}He + He‡	$7.0^{+0.2}_{-0.3}$	$0.31^{+0.03}_{-0.02}$	-	74^{+4}_{-3}	$2.36^{+0.03}_{-0.01}$	$0.43^{+0.08}_{-0.05}$	4.6
^{2}H/^{4}He + ^{2}H + He	$14.8^{+0.5}_{-0.5}$	$0.08^{+0.03}_{-0.03}$	-	44^{+5}_{-8}	$2.66^{+0.03}_{-0.03}$	$0.70^{+0.05}_{-0.03}$	5.6
B/C [Putze et al., 2010]	$9.7^{+0.3}_{-0.2}$	$0.234^{+0.006}_{-0.005}$	-	73^{+2}_{-2}	$\alpha + \delta = 2.65$	-1	4.7
B/C [this paper]	$6.2^{+0.4}_{-0.3}$	$0.35^{+0.01}_{-0.01}$	-	80^{+2}_{-2}	$[1.8, 2.5]$	$[-2, +2]$	1.5
B/C + C (all) [this paper]	$6.5^{+0.1}_{-0.1}$	$0.314^{+0.006}_{-0.006}$	-	57^{+2}_{-1}	$2.340^{+0.005}_{-0.008}$	$0.96^{+0.04}_{-0.04}$	13.9
B/C + C (HEAO) [this paper]	$6.3^{+0.1}_{-0.1}$	$0.353^{+0.004}_{-0.004}$	-	78^{+1}_{-2}	$2.250^{+0.015}_{-0.006}$	$1.48^{+0.08}_{-0.12}$	2.8
Model III							
^{3}He/^{4}He	$0.5^{+0.4}_{-0.3}$	$0.67^{+0.04}_{-0.10}$	$27.4^{+0.9}_{-1.3}$	41^{+14}_{-8}	$[1.8, 2.5]$	$[-2, +2]$	2.9
^{3}He/^{4}He + ^{3}He + He‡	$1.0^{+0.3}_{-0.2}$	$0.64^{+0.03}_{-0.05}$	$23.5^{+0.5}_{-1.0}$	54^{+5}_{-3}	$2.37^{+0.03}_{-0.03}$	$0.03^{+0.04}_{-0.04}$	1.6
^{2}H/^{4}He + ^{2}H + He	$3.2^{+0.8}_{-0.1}$	$0.50^{+0.08}_{-0.10}$	$27.1^{+2.5}_{-1.8}$	72^{+9}_{-16}	$2.41^{+0.12}_{-0.08}$	$0.39^{+0.07}_{-0.06}$	5.5
B/C [Putze et al., 2010]	$0.46^{+0.08}_{-0.06}$	$0.86^{+0.04}_{-0.04}$	$18.9^{+0.3}_{-0.4}$	38^{+2}_{-2}	$\alpha + \delta = 2.65$	-1	1.5
B/C [this paper]	$0.46^{+0.18}_{-0.10}$	$0.82^{+0.08}_{-0.05}$	$18.3^{+0.2}_{-0.3}$	40^{+5}_{-4}	$[1.8, 2.5]$	$[-2, +2]$	0.9
B/C + C (all) [this paper]	$0.57^{+0.05}_{-0.03}$	$0.80^{+0.02}_{-0.01}$	$17.4^{+0.2}_{-0.3}$	36^{+1}_{-1}	$2.260^{+0.007}_{-0.009}$	$0.24^{+0.03}_{-0.05}$	5.2
B/C + C (HEAO) [this paper]	$0.33^{+0.06}_{-0.10}$	$0.93^{+0.05}_{-0.07}$	$18.2^{+0.3}_{-0.2}$	35^{+4}_{-2}	$2.312^{+0.019}_{-0.008}$	$1.9^{+0.1}_{-0.2}$	2.0

‡ Excluding PAMELA He point below 5 GeV/n and above 183 GeV/n.

Note 5. An interval in square brackets corresponds to the prior used for the analysis (the posterior PDF obtained is close to the prior).

Note 6. The B/C results are based on IMP7-8 (Garcia-Munoz et al. 1987), Voyager 1&2 (Lukasiak et al. 1999), ACE-CRIS (George et al. 2009), HEA0-3 (Engelmann et al. 1990), Spacelab (Mueller et al. 1991), AMS-01 (Aguilar et al. 2011), and CREAM (Ahn et al. 2008), shown to be the most compatible data for a B/C analysis (Putze et al. 2009).

4.3. MCMC analysis: 'best' results

Taking into account specificities of the actual data (previous section), our 'best' analysis is based on the most relevant combinations of data for ^{2}H and ^{3}He:

- the ^{3}He/^{4}He analysis (with a prior for the source parameters) gives robust and conservative results for the transport parameters. The result from the ^{3}He/^{4}He+^{3}He+He‡ analysis is more sensitive to biases, but using an energy sub-range for He data is expected to limit them.
- Due to the paucity of ^{2}H data, the ^{2}H/^{4}He+^{2}H+He (full energy-range for He) analysis is the only reliable option, although it probably suffers from biases.

The corresponding most-probable values and CIs are gathered in Table 5, and the corresponding envelopes for ^{2}H/^{4}He, ^{2}H, ^{3}He/^{4}He, and ^{3}He/^{4}He are given in Fig. 4. We also re-analyse the B/C ratio according to our 'best-analysis' scheme (B/C alone with a prior for the source parameters or B/C + C). The results are reported in Table 5, where the results obtained in Putze et al. (2010) for fixed source parameters are also reproduced: we note that the new strategy gives results in better agreement with those of the quartet analysis (e.g., the transport parameters δ and K_0 are shifted by more than 30% for Model II), further demonstrating its usefulness.

4.3.1. Universality of the transport parameters

If we focus on the transport parameters, we note that combinations involving the ^{2}H/^{4}He, ^{3}He/^{4}He, or B/C ratio give broadly consistent transport parameter values, be it for Model II or Model III[10]. Regardless of the actual propagation model, we conclude that these results hint at the universality of CR transport for all species. Another important result is that the constraints set by the quartet data on the transport parameters are competitive with those set by the B/C ratio, so that the quartet data should be a prime target for AMS-02.

4.3.2. Model II ($\delta \sim 0.3$) or Model III ($\delta \sim 0.7$)?

According to Sect. 3.2, comparing the results of the secondary-to-primary ratio analysis with those of the combined analysis (ratio + primary flux) gives an indication of their robustness. Table 5 show that the results for the diffusion slope δ is very robust, regardless of the model considered. A more detailed comparison shows that for ^{3}He-related constraints, the transport parameter values for Model II are inconsistent with one another at the 3σ level, whereas the 68% CIs overlap with one another (but for V_c)

[10] The most significant difference is for the ^{2}H/^{4}He+^{2}H+He analysis, which is inconsistent in both models and clearly unreliable for Model II ($\delta \sim 0$). For model III, B/C and ^{3}He/^{4}He-related constraints are roughly in the same region but are located at several σ from each others (they are consistent with one another for Model II).

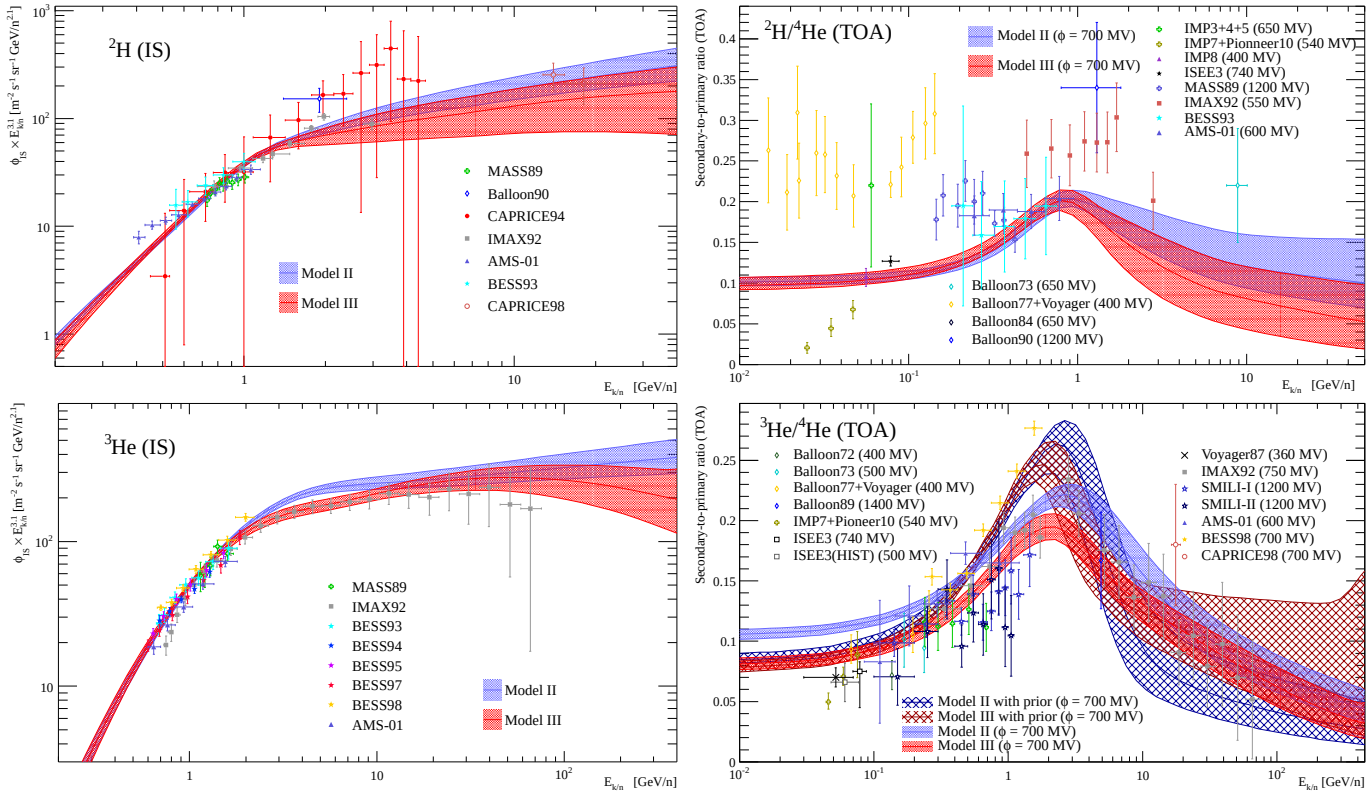


Fig. 4. Left panels: demodulated interstellar ^{2}H (top) and ^{3}He (bottom) envelopes at 95% CIs times $E_{k/n}^{3.1}$. Right panels: top-of-atmosphere secondary-to-primary ratio ^{2}H/^{4}He (top) and ^{3}He/^{4}He (bottom) ratios. The full envelopes correspond to the 'best' simultaneous analysis (secondary-to-primary ratio + primary flux) for model II (blue) and III (red). The hatched envelopes correspond to the ^{3}He/^{4}He analysis (prior on source parameters). See Table A.1 for references and the corresponding demodulation (for IS) and modulation (TOA) level ϕ.

for Model III, hence slightly favouring the latter ($\delta \sim 0.7$). The comparison of the $\chi^2_{\rm best}$/d.o.f. values also tends to favour model III. Hence, although the value $\delta \sim 0.7$ seems favoured, we cannot exclude yet pure reacceleration model ($V_c = 0$) with $\delta \sim 0.3$. Moreover, as shown in Maurin et al. (2010), many ingredients of the propagation models can lead to a systematic scatter of the transport parameters larger than the width of their CIs. Data at higher energy for any secondary-to-primary ratio are mandatory to conclude on this issue.

4.3.3. Source spectrum

The present analysis is more general than that used in Putze et al. (2011), where the transport parameters were fixed. Although it is not the main focus of this paper, we remark that the values of the source slope α from the B/C + C analysis are consistent with those found in Putze et al. (2011), strengthening the case of a universal source slope α at the $\sim 5\%$ level. For the quartet values, $\alpha_{\rm He}$ is broadly consistent with Putze et al.'s analysis (based on AMS-01, BESS98 and BESS-TeV data for He). However, the results for the source parameters depend on the choice of data sets and energy-range considered. This indicates that for $\lesssim 1\%$ accuracy data, either the model for the source is inappropriate, or the solar modulation model is faulty, or some systematics exist in the measurements. The AMS-02 data will help to clarify this question.

5. Conclusion

We have revisited the constraints set on the transport (and also the source) parameters by the quartet data, i.e. ^{1}H, ^{2}H, ^{3}He, and ^{4}He fluxes, but also the secondary-to-primary ratios ^{2}H/^{4}He and ^{3}He/^{4}He. This extends and complements a series of studies (Putze et al. 2009, 2010, 2011) carried out with the USINE propagation code and an MCMC algorithm. The three main ingredients on which the analysis rests are:

- A minute compilation of the existing quartet data and survey of the literature, showing that the most recent/precise data (AMS-01, BESS93→98, CAPRICE98, IMAX92, and SMILI-II) have not been considered before this analysis.
- We have done a systematic survey of the literature for the cross-sections involved in the production/survival of the quartet nuclei. This has lead us to propose new empirical production cross-sections of ^{2}H, ^{3}H, and ^{3}He, valid above a few tens of MeV/n, for any projectile on p and He (we also updated inelastic cross-sections).
- We have made an extensive use of artificial data sets to assess the reliability of the derived CIs of the GCR transport and source parameters for various combinations of data/parameters analyses.

In broad agreement with previous studies, (e.g. Ramaty & Lingenfelter 1969; Beatty 1986), we find that the fragmentation of CNO contributes significantly to the

^{2}H flux ($\sim 30\%$) above a few GeV/n energies (^{4}He fragmentation is the dominant channel for the ^{2}H and ^{3}He fluxes). Nevertheless, we provide a much finer picture, showing in particular that heavy nuclei ($8 < Z \leq 30$) contribute up to 10% for ^{3}He (20% for ^{2}H) at high energy. We also provide an estimate of the secondary fraction to the ^{4}He flux. By definition, the secondary contribution has a steeper spectrum than the primary one and therefore becomes quickly negligible at high energy. This secondary contribution peaks at a few GeV/n, and it amounts to $\sim 10\%$ of the total flux ($\sim 7\%$ up to O fragmentation, $\sim 2\%$ from elements heavier than O), which is already a sizeable amount given the $\sim 1\%$ precision reached by the PAMELA data (Adriani et al. 2011). For ^{1}H, the knowledge of the multiplicity of neutron and proton produced by the interaction of all elements on the ISM is required to calculate precisely its secondary content.

Simulated data have allowed us to check several critical behaviours. Firstly, the He flux is obviously useful (and required) to constrain the source parameters, but it has also been found to bring significant information on the transport parameters: fitting a secondary-to-primary ratio plus a primary flux brings more constraints than just fitting the ratio (even when source parameters are fixed). Secondly, we have checked that a model with more free parameters (than the ones used to simulate the data) is able to recover the correct values. However, our analysis has also strongly hinted at the fact that adding the primary flux He biases the determination of the transport parameters if systematics (which are usually more important in primary fluxes than in ratios) are present, and/or if the wrong model is used. For this reason, when dealing with measurements, we recommend to always compare the result from the *secondary-to-primary ratio + primary flux* analysis to that of the *secondary-to-primary ratio* using a loose but physically motivated prior on the source parameters.

The analysis of real data has shown that quartet data slightly favours a model with large $\delta \sim 0.7$ (with $V_c \sim 20$ km s^{-1} and $V_a \sim 40$ km s^{-1}), but that a model with small $\delta \sim 0.2$ (with $V_c \sim 0$ and $V_a \sim 80$ km s^{-1}) cannot be completely ruled out. Better quality data, and especially data at higher energy are required to go further. The conclusions are similar and the range of transport parameters found are consistent with those obtained from the B/C analysis (Jones et al. 2001; Putze et al. 2010; Maurin et al. 2010)[11]. This strongly hints at the the universality of the GCR transport for any all nuclei. Furthermore, we have shown that the analysis of the light isotopes (and the already very good precision on He) is as constraining as the B/C analysis (similar range of CIs).

The several difficulties which have been pointed out in this analysis could be alleviated by virtue of using better data. However, it is more likely that the interpretation of future high-precision data will require the development of refined models for the source spectra and/or transport and/or solar modulation. For instance, the Force-Field approximation for solar modulation is already too crude to minutely match the PAMELA He data. The forthcoming AMS-02 data at an even better accuracy will definitively pose interesting new challenges.

Acknowledgements. D. M. would like to thank A. V. Blinov for kindly providing copies of several of his articles. A. P. is grateful for financial support from the Swedish Research Council (VR) through the Oskar Klein Centre.

Appendix A: Cosmic-ray data

Deuterons and ^{3}He fluxes are very sensitive to the modulation level, whereas ratios are less affected. The exact value for the solar modulation level ϕ is uncertain. For instance, the values given in the seminal papers can differ greatly from those estimated by Casadei & Bindi (2004) (in order to match the electron and positron fluxes of various experiments, see their Table 1), or from those reconstructed from the Neutron monitors (Usoskin et al. 2002). This difference may be attributed to the fact that the latter analysis correctly solves the Fokker-Plank equation of GCR transport in the Heliosphere, whereas most papers rely on the widely used force-field approximation that is known to fail for strong modulation level $\phi \gtrsim 1000$ MV (e.g., Usoskin et al. 2002). In this analysis, we do not attempt to go beyond this force-field approximation, as speed is of essence for our MCMC analysis. We rely mostly on the force-field effective modulation parameter ϕ necessary to reproduce the data (as quoted in the seminal paper), but these values are slightly adjusted in order to give overlapping fluxes when all the data are demodulated and plotted together. Given the uncertainty on the data, the large uncertainty on ϕ, and the fact that most-probable region of parameter space is constrained by the ^{2}H/^{4}He and ^{3}He/^{4}He ratio (rather than the best fit to the ^{2}H and ^{3}He fluxes), we feel that it is a safe procedure till high precision data from PAMELA of AMS-02 are available.

The demodulated interstellar (IS) fluxes for ^{2}H and ^{3}He are shown in the left panels of Fig. 4, whereas the yet modulated top-of-atmosphere (TOA) ratios for ^{2}H/^{4}He and ^{3}He/^{4}He are shown in its right panels. The references for the data are given in Table A.1.

Appendix B: Cross-sections

This appendix summarises the production and destruction cross-sections employed for the quartet nuclei in this paper.

B.1. Elastic and inelastic cross-sections

All reaction cross-sections are taken from the parametrisations of Tripathi et al. (1999), but for the pH reaction cross-section. The latter is evaluated from $\sigma_{\rm pp}^{\rm inel} = \sigma_{\rm pp}^{\rm tot} - \sigma_{\rm pp}^{\rm el}$, where the total and elastic cross-sections are fitted to the data compiled in the PDG[12]. Note also that for ^{4}He $+^4$ He, we had to renormalise Tripathi et al. (1999) formulae by a factor 0.9 to match the low-energy data.

Our parametrisations (lines) and the data (symbols) are shown in Fig. B.1 for reaction on H and He. Note that we rely on Tripathi et al. (1997) for any other inelastic reaction.

[11] Note that in this paper, we did not attempt to combine the results of different secondary-to-primary ratios (^{2}H/^{4}He, ^{3}He/^{4}He, B/C, sub-Fe/Fe, $\bar{p}/p$). This is left for a future study, for which a Bayesian evidence could be used to better address (in a Bayesian framework) the crucial issue of model selection.

[12] `http://pdg.lbl.gov/`

Table A.1. References for the quartet data.

Exp.	#data	Year	ϕ (MV)	Ref.	Comment
				— ^{2}H —	
MASS89	9	1989	1200	Webber et al. (1991)	
Voyager87	7	1987	360	Seo et al. (1994)	Voyager is at 23 AU
Balloon90	1	1990	1200	Bogomolov et al. (1995)	
Voyager94	4	1994	150	Seo & McDonald (1995)	Voyager is at 56 AU
CAPRICE94	14	1994	600	Boezio et al. (1999)	Subtraction of H to ^{1}H from Tab 3.
IMAX92	8	1992	550	de Nolfo et al. (2000)	
AMS-01	10	1998	600	AMS Collaboration (2002)	
BESS93	5	1993	700	Wang et al. (2002)	
CAPRICE98	5	1998	700	Papini et al. (2004)	
				— ^{3}He —	
MASS89	5	1989	1200	Webber et al. (1991)	
Voyager87	7	1987	360	Seo et al. (1994)	Voyager is at 23 AU
Voyager94	4	1994	150	Seo & McDonald (1995)	Voyager is at 56 AU
IMAX92	24	1992	750	Menn et al. (2000)	
BESS93	7	1993	700	Wang et al. (2002)	
BESS94	5	1994	630	Myers et al. (2003)	Taken from their Fig. 2
BESS95	6	1995	550	Myers et al. (2003)	Taken from their Fig. 2
BESS97	7	1997	491	Myers et al. (2003)	Taken from their Fig. 2
BESS98	7	1998	700	Myers et al. (2003)	Taken from their Fig. 2
AMS-01	5	1998	600	Aguilar et al. (2011)	
				— ^{2}H/^{4}He —	
IMP3+4+5	1	65+67+69	650	Hsieh et al. (1971)	
Balloon73	1	1973	650	Apparao (1973)	
IMP7+Pioneer10	3	72+73	540	Teegarden et al. (1975)	
Balloon77+Voyager	14	1977	400	Webber & Yushak (1983)	
IMP8	1	1977	400	Beatty et al. (1985)	
ISEE3	1	78-84	740	Kroeger (1986)	
Balloon84	1	1974	650	Durgaprasad & Kunte (1988)	(discarded in the analysis)
MASS89	9	1989	1200	Webber et al. (1991)	
Balloon90	1	1990	1200	Bogomolov et al. (1995)	
IMAX92	8	1992	550	de Nolfo et al. (2000)	
AMS-01	4	1998	600	Aguilar et al. (2011)	
				— ^{3}He/^{4}He —	
Balloon72	2	1972	400	Webber & Schofield (1975)	Re-analysed by Webber et al. (1987)
IMP7+Pioneer10	2	72+73	540	Teegarden et al. (1975)	
Balloon73	2	1973	500	Leech & Ogallagher (1978)	
Balloon77+Voyager	3	1977	400	Webber & Yushak (1983)	Re-analysed by Webber et al. (1987)
Balloon81	1	1981	440	Jordan (1985)	(discarded, see Webber et al. 1987)
ISEE3	2	78-84	740	Kroeger (1986)	
ISEE3(HIST)	1	78	500	Mewaldt (1986)	
MASS89	5	1989	1200	Webber et al. (1991)	
SMILI-I	12	1989	1200	Beatty et al. (1993)	
Voyager87	1	1987	360	Seo et al. (1994)	Voyager is at 23 AU
Balloon89	1	1989	1400	Hatano et al. (1995)	
IMAX92	21	1992	750	Menn et al. (2000)	
SMILI-II	10	1991	1200	Ahlen et al. (2000)	
BESS98	7	1998	700	Myers et al. (2003)	
CAPRICE98	1	1998	700	Mocchiutti et al. (2003)	
AMS-01	5	1998	600	Aguilar et al. (2011)	Supersedes Xiong et al. (2003) data

B.2. Light nuclei production: Nuc + p

The light nuclei ^{3}He and ^{2}H are spallative products of cosmic rays interacting with the interstellar medium (ISM). The total secondary flux is obtained from the combination of production cross-sections and measured primary fluxes. In principle, all nuclei must be considered, but the ISM and GCRs are mostly composed of ^{1}H and ^{4}He, making the reactions involving these species dominant. For heavier species, their decreasing number is balanced by their higher cross-section. In several studies (e.g. Ramaty & Lingenfelter 1969; Jung et al. 1973b; Beatty 1986), it was found that the CNO_{CR}+ H_{ISM} reactions contribute to $\sim$ 30% of the ^{2}H flux above GeV/n energies. The reverse reaction H_{CR}+CNO_{ISM} mostly produces fragments at lower energies, making them irrelevant

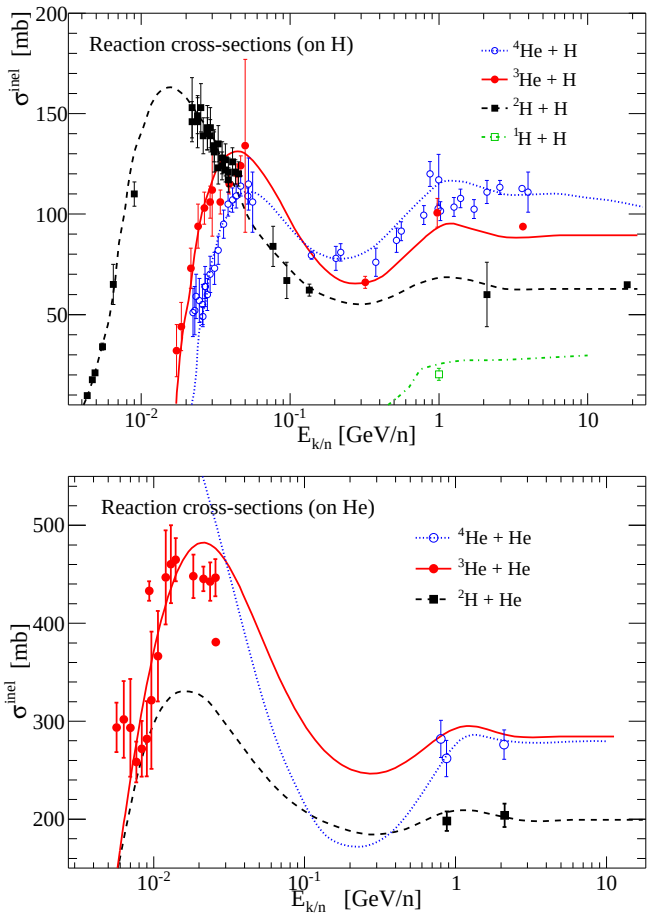


Fig. B.1. Total inelastic (reaction) cross-section for the quartet isotopes. The lines show our parametrisation (see text), the symbols are data. **Top panel:** reaction on H with data from Cairns et al. (1964); Hayakawa et al. (1964); Igo et al. (1967); Palevsky et al. (1967); Griffiths & Harbison (1969); Nicholls et al. (1972); Carlson et al. (1973); Sourkes et al. (1976); Ableev et al. (1977); Klem et al. (1977); Jaros et al. (1978); Velichko et al. (1982); Blinov et al. (1984, 1985); Abdullin et al. (1993); Glagolev et al. (1993); Webber (1997). **Bottom panel:** reaction on He with data from Koepke & Brown (1977); Jaros et al. (1978); Tanihata et al. (1985).

for CR studies in the regime $\gtrsim$ 100 MeV/n[13]. Note that ^{3}H is also produced in these reactions, but it decays in ^{3}He with a life time (12.2 years) short with respect to the propagation time. All tritium production is thus assimilated to ^{3}He production, but the cross-sections for this fragment are provided as well below.

The energy of the fragments roughly follows a Gaussian distribution (e.g. Cucinotta et al. 1993). Its impact on the secondary flux was inspected for the B/C analysis by Tsao et al. (1995), where an effect $\lesssim 10\%$ was found, compared to the straight-ahead approximation, in which the kinetic energy per nucleon of the fragment equals that of the projectile. The precision sought for the cross-sections is driven by the level of precision attained by the CR data to analyse. Given the large errors on the existing data, the straight-ahead approximation is enough for this analysis. However, future high-precision data (e.g. from the AMS-02 experiment) will probably require a refined description.

[13] Solar modulation also ensures that only species created at energies $\gtrsim$ GeV/n matter.

B.2.1. ^{4}He + p $\rightarrow$ ^{2}H, ^{3}H, and ^{3}He

Recent and illustrative reviews on ^{4}He+H reaction and the production of light fragments is given by Bildsten et al. (1990); Cucinotta et al. (1993); Blinov & Chadeyeva (2008). As said earlier, we are only interested in the total inclusive production cross-section, not in all the possible numerous final states (see, e.g., Table 3 of Blinov & Chadeyeva 2008). We adapt the parametrisation of Cucinotta et al. (1993), which takes into account separately the break-up and stripping (for ^{3}He and ^{2}H) cross-sections. The former reaction corresponds to the case where the helium nucleus breaks up leading to coalescence of free nucleons into a new nucleus. The latter happens via the pickup reaction where the incident proton tears a neutron or a proton off the helium nucleus. Both reaction and the total are shown along with the experimental data in Fig. B.2.

The most accurate set of data (upward blue empty triangles) are from the experiments set up in ITEP and LHE JINR (Aladashvill et al. 1981; Glagolev et al. 1993; Abdullin et al. 1994, summarised in Blinov & Chadeyeva 2008). Their highest energy data point (Glagolev et al. 1993) is a conservative estimate as the more or equal to 6-prong reactions are not detailed (see Table 3 of Blinov & Chadeyeva 2008 and Table 4 of Glagolev et al. 1993). To take into account that possibility, we consider an error of a few mb in the plots of Fig. B.2. Let us consider in turn each product of interest.

^{3}He production The stripping cross-section data (d and ^{3}He in the final state) are well fitted by Eq. (130) of Cucinotta et al. (1993). However, the Griffiths & Harbison (1969) and (Jung et al. 1973a) are $\sim 30\%$ below the other data. Actually, for the latter (filled stars) the break-up cross-section is above other data, it may be that the end products are misreconstructed (in this or the other experiments). Nevertheless, the sum of the two—which is the one that matters—is consistent in all data. Note that we slightly modified the break-up cross-section provided by Cucinotta et al. (1993) to better fit the high-energy data points. For the latter, all the data are consistent with one another, but for the high precision ITEP data at 200 MeV/n.

^{2}H production The stripping cross-section is as for ^{3}He (d and ^{3}He in the final state). The high-energy break-up cross-section data (LHE JINR and Webber 1990b) are inconsistent. We have decided to rescale the Webber data, to take into account the fact that in his preliminary account of the results (Webber 1990b), the total inelastic cross-section is smaller than that given in a later and updated study (Webber 1997). Still, the agreement between the two sets is not satisfactory. The other high-energy data point is the Innes (1957) experiment, and it suffers large uncertainties and maybe systematics (it is for n + ^{4}He reaction, and the data point is provided by Meyer (1972) who relied on

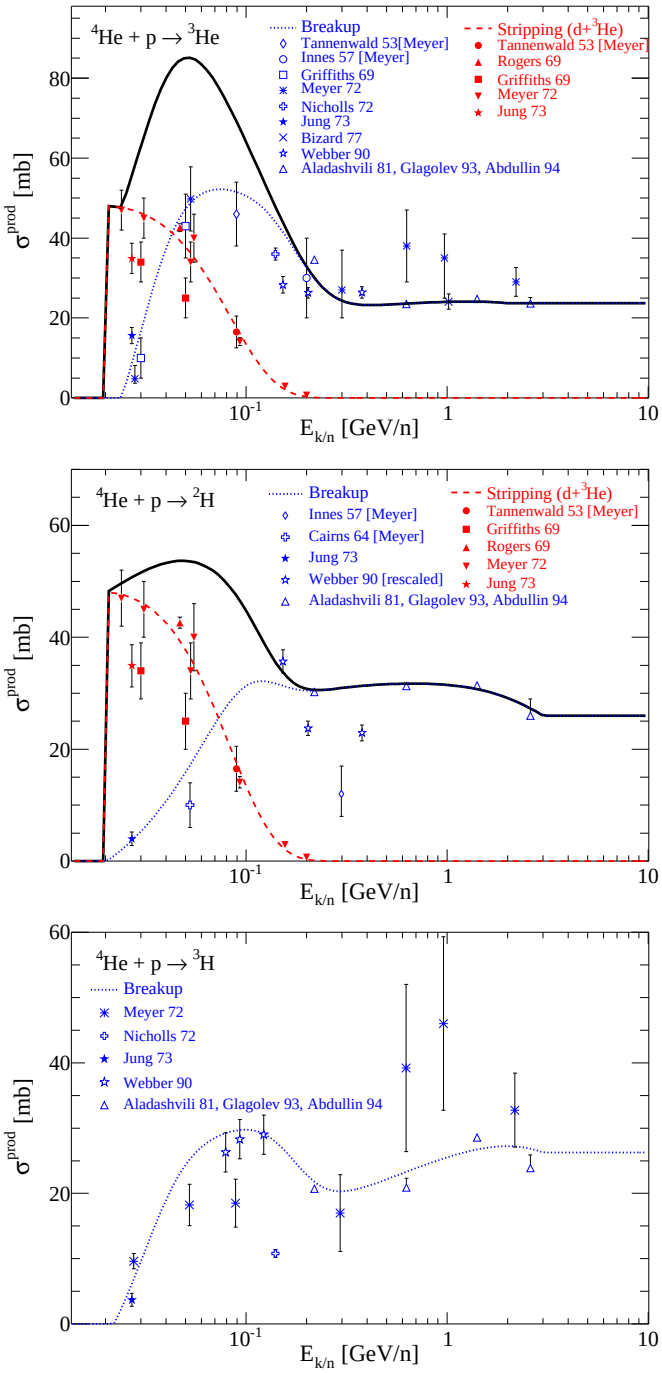


Fig. B.2. Inclusive production cross-sections of ^{3}He (top), ^{2}H (centre) and ^{3}H (bottom) in ^{4}He+H reaction. The data (see text for details) are from Tannenwald (1953); Innes (1957); Cairns et al. (1964); Rogers et al. (1969); Griffiths & Harbison (1969); Meyer (1972); Jung et al. (1973a); Aladashvill et al. (1981); Webber (1990b); Glagolev et al. (1993); Abdullin et al. (1994).

several assumptions to get it). The ITEP/LHE JINR data being the best available, we have replaced the formula for the ^{2}H breakup of Cucinotta et al. (1993) by a form similar as that given for ^{3}He, but where we changed the parameters to fit the high energy points.

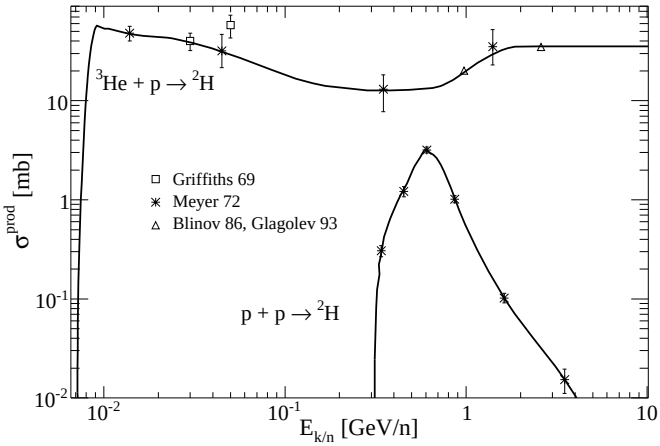


Fig. B.3. ^{2}H other production channels from the less abundant ^{3}He and the peaked fusion pp reaction (the much smaller cross-section is redeemed by a CR flux higher (p instead of ^{3}He). The data are from Griffiths & Harbison (1969); Meyer (1972); Blinov et al. (1986); Glagolev et al. (1993).

^{3}H production There is only break-up for the Cucinotta et al. (1993) ^{3}H production. The data are in broad agreement with one another, but for the Nicholls et al. (1972) point (open plus). Again, we have adapted the Cucinotta et al. (1993) parametrisation to better fit the ITEP/LHE JINR data.

B.2.2. ^{3}He + p → ^{2}H (breakup) and p + p → ^{2}H (fusion)

There are two other channels for producing ^{2}H from light nucleus reactions, and they are shown in Fig. B.3 along with the data. The first one is from ^{3}He (break-up and stripping). The CR flux of the latter is less abundant than the ^{4}He flux. With a ratio of $\sim 20\%$ at 1 GeV/n (decreasing at higher energy) and similar production cross-sections ($\sim 30 - 40$ mb), this is expected to contribute by the same fraction at GeV/n energies, and then to become negligible $\gtrsim 10$ GeV/n. The second channel is the ^{2}H coalescence from two protons. The cross-section is non-vanishing only for a very narrow energy range. Even if the cross-section is 10 times smaller than for the other channels, the fact that CR protons are ~ 10 times more numerous than ^{4}He makes it a significant channel slightly below 1 GeV/n.

The fitting curves are taken from Meyer (1972), but we adapted the fit for the ^{3}He+p channel to match the two high-energy ITEP/LHE JINR data points.

B.2.3. Proj$_{(A>4)}$ + p → ^{2}H, ^{3}H, and ^{3}He

For nuclear fragmentation cross-sections of heavier nuclei, the concepts of 'strong' or 'weak' factorisation relies on the fact that at high energy enough, the branching of the various outgoing particles-production channels becomes independent of the target. This corresponds to the factorisation $\sigma^{\rm strong}(P,F,T) = \gamma_{\rm P}^{\rm F}\,\gamma_{\rm T}$ or $\sigma^{\rm weak}(P,F,T) = \gamma_{\rm P}^{\rm F}\,\gamma_{\rm PT}$ where $\sigma(P,F,T)$ is the fragmentation cross-section for the projectile P incident upon the target T producing the fragment F. This is discussed, e.g., in Olson et al. (1983), where it

is concluded that although strong factorisation is probably violated, weak factorisation seems exact (see also, e.g., Michel et al. 1995). The parametrisation proposed below takes advantage of it.

Several data exist for the production of light isotopes from nuclei $A \geq 12$ on H (see Table B.1). The most complete sets of data in terms of energy coverage are for the projectiles C, N, and O ($\langle A \rangle = 14$), the group Mg, Al, and Si ($\langle A \rangle = 26$), and the group Fe and Ni ($\langle A \rangle = 57$). They are plotted in Fig. B.4 (top panels and bottom left panel). The solid lines correspond to an adjustment (by eye), rescaled from the $\sigma^{^4\mathrm{Hep}\rightarrow^3\mathrm{He}}_{\mathrm{breakup}}$ cross-section (because heavy projectile do not give $A = 3$ fragments in the stripping process). As $\sigma^{\mathrm{prod}}_{^3\mathrm{He}} \approx \sigma^{\mathrm{prod}}_{^3\mathrm{H}}$, no distinction is made for the fit (^{2}H data are scarce and do not influence the conclusions drawn from these three groups of nuclei). The following parametrisation

$$\sigma^{\mathrm{Pp}\rightarrow\mathrm{F}}(E_{k/n}, A_{\mathrm{P}}) = \gamma^{\mathrm{F}}_{\mathrm{P}} \cdot f(E_{k/n}, A_{\mathrm{P}}) \cdot \sigma^{^4\mathrm{Hep}\rightarrow^3\mathrm{He}}_{\mathrm{breakup}}(E_{k/n}) \ , \tag{B.1}$$

with

$$f(E_{k/n}, A_{\mathrm{P}}) = \begin{cases} \left(\frac{E_{k/n}}{1.5\ \mathrm{GeV/n}}\right)^{0.8\cdot\sqrt{\frac{A_{\mathrm{P}}}{26}}} & \text{if } E_{k/n} < 1.5\ \mathrm{GeV/n}, \\ 1 & \text{otherwise;} \end{cases} \tag{B.2}$$

proves to fit well the three groups of data for energies greater than a few tens of MeV/n. Thanks to the $f(E_{k/n}, A_{\mathrm{proj}})$ factor, there is no further energy dependence in the $\gamma^{\mathrm{F}}_{\mathrm{P}}$ factor, so that the latter can be determined from the data points at any energy. The bottom right panel of Fig. B.4 shows the measured mean value and dispersion[14] as a function of A, from which we obtain:

$$\begin{aligned} \gamma^{^3\mathrm{He}}_{\mathrm{P}} &= \gamma^{^3\mathrm{H}}_{\mathrm{P}} = 1.3 \left[1 + \left(\frac{A_{\mathrm{P}}}{25}\right)^{1.5}\right], \\ \gamma^{^2\mathrm{H}}_{\mathrm{P}} &= 0.28\, A_{\mathrm{P}}^{1.2}. \end{aligned} \tag{B.3}$$

The set of formulae (B.1), (B.2), and (B.3) completely define the Proj+p production cross-sections for the light fragments.

B.3. Proj$_{(A\geq4)}$ + ^{4}He → ^{2}H, ^{3}H, and ^{3}He

Data for T + ^{4}He where the target T is heavier than p are scarce. In a compilation of Davis et al. (1995), the authors find that the ^{3}He production scales as $A_{\mathrm{T}}^{0.31}$ (based on 4 data point with $A_{\mathrm{T}} \geq 7$). This is the scaling we employ for the ^{3}H and ^{2}H production as well.

References

Abdullin, S. K., Blinov, A. V., Chadeeva, M. V., et al. 1994, Nuclear Physics A, 569, 753
Abdullin, S. K., Blinov, A. V., Vanyushin, I. A., et al. 1993, Physics of Atomic Nuclei, 56, 536
Ableev, V. G. et al. 1977, JINR-P1-10565
Adriani, O. et al. 2011, Science, 332, 69
Aguilar, M. et al. 2011, ApJ, 736, 105
Ahlen, S. P., Greene, N. R., Loomba, D., et al. 2000, ApJ, 534, 757
Ahn, H. S., Allison, P., Bagliesi, M. G., et al. 2010, ApJ, 714, L89
Ahn, H. S., Allison, P. S., Bagliesi, M. G., et al. 2008, Astroparticle Physics, 30, 133
Aladashvill, B., Bano, M., Braun, H., et al. 1981, Acta Physica Slovaca, 31, 29
Ammon, K., Leya, I., Lavielle, B., et al. 2008, Nuclear Instruments and Methods in Physics Research B, 266, 2
AMS Collaboration. 2002, Phys. Rep., 366, 331
Apparao, K. M. V. 1973, in International Cosmic Ray Conference, Vol. 1, International Cosmic Ray Conference, 126
Badhwar, G. D. & Daniel, R. R. 1963, Progress of Theoretical Physics, 30, 615
Beatty, J. J. 1986, ApJ, 311, 425
Beatty, J. J., Ficenec, D. J., Tobias, S., et al. 1993, ApJ, 413, 268
Beatty, J. J., Garcia-Munoz, M., & Simpson, J. A. 1985, ApJ, 294, 455
Bieri, R. H. & Rutsch, W. 1962, Helv. Phys. Acta, 35, 553
Bildsten, L., Wasserman, I., & Salpeter, E. E. 1990, Nuclear Physics A, 516, 77
Blinov, A. V. & Chadeyeva, M. V. 2008, Physics of Particles and Nuclei
Blinov, A. V. et al. 1984, Yad. Fiz., 39, 260
Blinov, A. V. et al. 1985, Sov. J. Nucl. Phys., 42, 133
Blinov, A. V. et al. 1986, Nucl. Phys., A451, 701
Boezio, M., Carlson, P., Francke, T., et al. 1999, ApJ, 518, 457
Bogomolov, E. A., Vasilyev, G. I., Yu, S., et al. 1995, in International Cosmic Ray Conference, Vol. 2, International Cosmic Ray Conference, 598
Cairns, D. J. et al. 1964, Nuc. Phys., 60, 369
Carlson, R. F. et al. 1973, Lett. Al Nuovo Cimento, 8, 319
Casadei, D. & Bindi, V. 2004, ApJ, 612, 262
Cucinotta, F. A., Townsend, L. W., & Wilson, J. W. 1993, Nasa technical report, L-17139; NAS 1.60:3285; NASA-TP-3285
Currie, L. A. 1959, Physical Review, 114, 878
Currie, L. A., Libby, W. F., & Wolfgang, R. L. 1956, Physical Review, 101, 1557
Davis, A. J., Menn, W., Barbier, L. M., et al. 1995, in International Cosmic Ray Conference, Vol. 2, International Cosmic Ray Conference, 622
de Nolfo, G. A., Barbier, L. M., Christian, E. R., et al. 2000, in American Institute of Physics Conference Series, Vol. 528, Acceleration and Transport of Energetic Particles Observed in the Heliosphere, ed. R. A. Mewaldt, J. R. Jokipii, M. A. Lee, E. Möbius, & T. H. Zurbuchen , 425–428
di Bernardo, G., Evoli, C., Gaggero, D., Grasso, D., & Maccione, L. 2010, Astroparticle Physics, 34, 274
Drury, L. O. 1983, Reports on Progress in Physics, 46, 973
Durgaprasad, N. & Kunte, P. K. 1988, A&A, 189, 51
Engelmann, J. J., Ferrando, P., Soutoul, A., Goret, P., & Juliusson, E. 1990, A&A, 233, 96
Evoli, C., Gaggero, D., Grasso, D., & Maccione, L. 2008, Journal of Cosmology and Astro-Particle Physics, 10, 18
Fireman, E. L. 1955, Physical Review, 97, 1303
Garcia-Munoz, M., Simpson, J. A., Guzik, T. G., Wefel, J. P., & Margolis, S. H. 1987, ApJSupp. Series, 64, 269
George, J. S., Lave, K. A., Wiedenbeck, M. E., et al. 2009, ApJ, 698, 1666
Glagolev, V. V. et al. 1993, Z. Phys., C60, 421
Goebel, H., Schultes, H., & Zähringer, J. 1964, CERN report (unpublished), No 64-12
Green, R. E. L., Korteling, R. G., & Jackson, K. P. 1984, Phys. Rev. C, 29, 1806
Griffiths, R. J. & Harbison, S. A. 1969, ApJ, 158, 711
Hatano, Y., Fukada, Y., Saito, T., Oda, H., & Yanagita, T. 1995, Phys. Rev. D, 52, 6219
Hayakawa, S. et al. 1964, J. Phys. Soc. Jpn, 19, 2004
Honda, M. & Lal, D. 1960, Physical Review, 118, 1618
Hsieh, K. C., Mason, G. M., & Simpson, J. A. 1971, ApJ, 166, 221
Igo, G. J. et al. 1967, Nuc. Phys. B, 3, 181
Innes, W. H. 1957, University of California Radiation Laboratory Report No. UCRL-8040 (unpublished)
Jaros, J., Wagner, A., Anderson, L., et al. 1978, Phys. Rev. C, 18, 2273
Jones, F. C. 1994, ApJS, 90, 561
Jones, F. C., Lukasiak, A., Ptuskin, V., & Webber, W. 2001, ApJ, 547, 264
Jordan, S. P. 1985, ApJ, 291, 207

[14] In practice, for a given A, the mean and dispersion are calculated from all the existing point above a projectile energy 150 MeV/n.

Table B.1. References for the light nuclei production cross-sections (references for ^{4}He projectiles are given in Fig. B.2).

Proj.	Frag.	#data	$E_{k/n}$	Ref.
N, O, Fe	^{3}H	3	2.2	Fireman (1955)
C, N, O, Mg, Al, Fe, Ni, Ag, Sn, Pb	^{3}H	26	0.45-6.2	Currie (1959); Currie et al. (1956)
C	^{3}H	4	0.225-0.73	Honda & Lal (1960)
Mg, Al	^{3}He	2	0.54	Bieri & Rutsch (1962)
C,O,Mg,Al,Si,V,Cr,Mn,Fe,Ni,Cu,Ag,Pb,Bi	^{3}H, ^{3}He	38	0.225-5.7	Goebel et al. (1964)
CNO	^{2}H, ^{3}H, ^{3}He	14	0.02-7.5	Ramaty & Lingenfelter (1969)
C, O, Si	^{3}H, ^{3}He	12	0.6-3.0	Kruger & Heymann (1973)
Si, Mg	^{3}He	33	0.02-0.06	Walton et al. (1976)
Mg	^{3}He	6	0.015-0.07	Pulfer (1979)
C, O	^{2}H, ^{3}H, ^{3}He	8	1.05-2.1	Olson et al. (1983)
Ag	^{3}He	1	0.48	Green et al. (1984)
Mg, Al, Si	^{3}He	3	0.6	Michel et al. (1989)
Mg, Al, Si, Fe, Ni	^{3}He	21	0.8-2.6	Michel et al. (1995)
Mg, Al, Si	^{3}He	33	0.015-1.6	Leya et al. (1998)
C	^{3}He	3	1.87-3.66	Korejwo et al. (2000, 2002)
Pb	^{3}He	22	0.04-2.6	Leya et al. (2008)
Fe, Ni	^{3}He	53	0.022-1.6	Ammon et al. (2008)

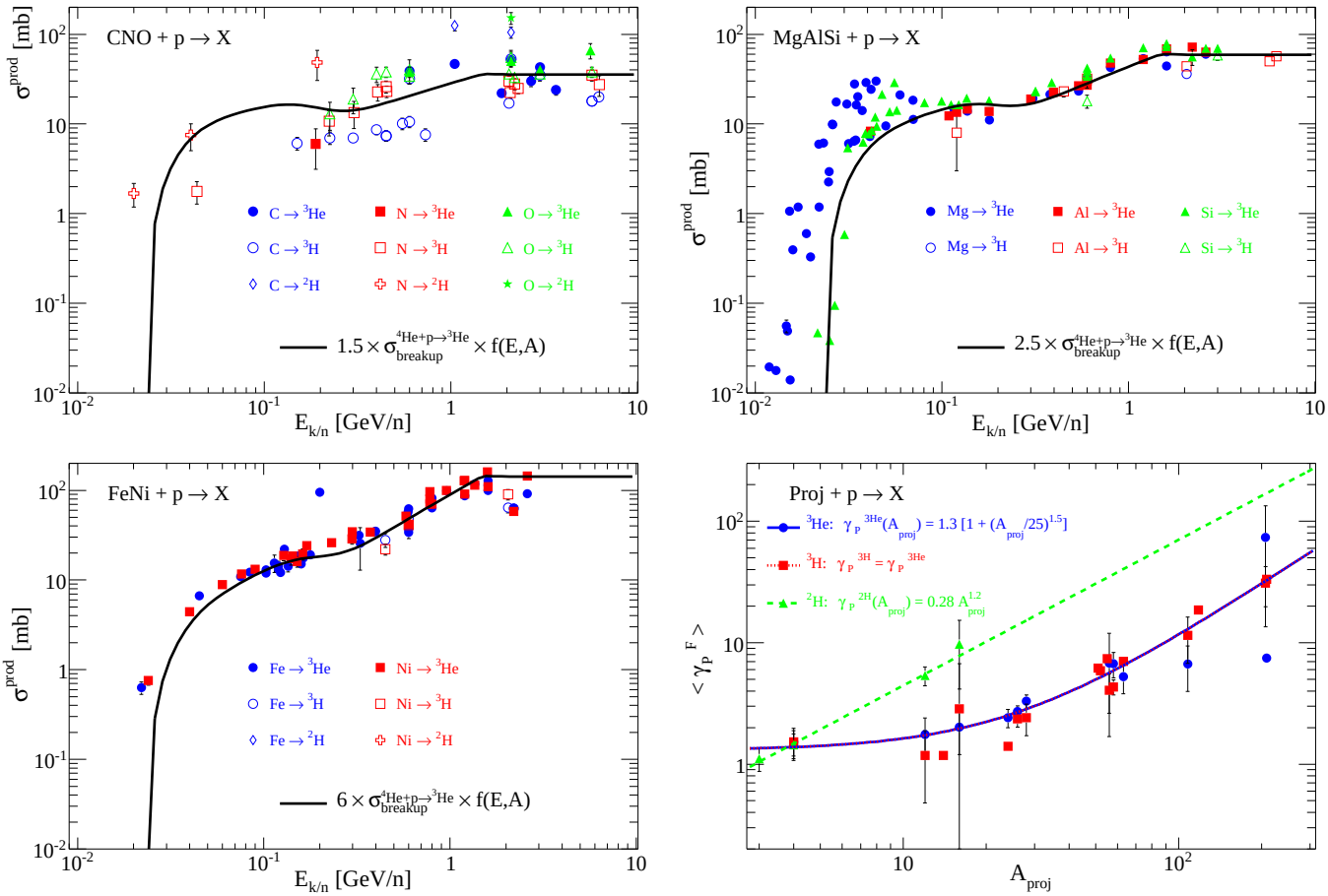


Fig. B.4. Proj$_{(A>4)}$ + p → ^{2}H, ^{3}H, and ^{3}He cross-sections for Proj=C,N,O (top left), Proj=Mg,Al,Si (top right), and Proj=Fe,Ni (bottom left). The bottom right correspond to the γ_P^F factor (see Eq. B.1 and text for explanations). The references for the data are gathered in Table B.1.

Jung, M., Sakamoto, Y., Suren, J. N., et al. 1973a, Phys. Rev. C, 7, 2209
Jung, M., Suren, J. N., Sakamoto, Y., et al. 1973b, in International Cosmic Ray Conference, Vol. 5, International Cosmic Ray Conference, 3086
Klem, R., Igo, G., Talaga, R., et al. 1977, Physics Letters B, 70, 155
Koepke, J. A. & Brown, R. E. 1977, Phys. Rev. C, 16, 18
Korejwo, A., Dzikowski, T., Giller, M., et al. 2000, Journal of Physics G Nuclear Physics, 26, 1171
Korejwo, A., Giller, M., Dzikowski, T., Perelygin, V. V., & Zarubin, A. V. 2002, Journal of Physics G Nuclear Physics, 28, 1199
Kroeger, R. 1986, ApJ, 303, 816

Kruger, S. T. & Heymann, D. 1973, Phys. Rev. C, 7, 2179
Leech, H. W. & Ogallagher, J. J. 1978, ApJ, 221, 1110
Leya, I., Busemann, H., Baur, H., et al. 1998, Nuclear Instruments and Methods in Physics Research B, 145, 449
Leya, I., David, J., Leray, S., Wieler, R., & Michel, R. 2008, Nuclear Instruments and Methods in Physics Research B, 266, 1030
Lionetto, A. M., Morselli, A., & Zdravkovic, V. 2005, Journal of Cosmology and Astro-Particle Physics, 9, 10
Lukasiak, A., McDonald, F. B., & Webber, W. R. 1999, 3, 41
Mannheim, K. & Schlickeiser, R. 1994, A&A, 286, 983
Maurin, D., Donato, F., Taillet, R., & Salati, P. 2001, ApJ, 555, 585
Maurin, D., Putze, A., & Derome, L. 2010, A&A, 516, A67
Menn, W., Hof, M., Reimer, O., et al. 2000, ApJ, 533, 281
Mewaldt, R. A. 1986, ApJ, 311, 979
Mewaldt, R. A., Stone, E. C., & Vogt, R. E. 1976, ApJ, 206, 616
Meyer, J. P. 1972, A&AS, 7, 417
Michel, R., Gloris, M., Lange, H., et al. 1995, Nuclear Instruments and Methods in Physics Research B, 103, 183
Michel, R., Peiffer, F., Theis, S., et al. 1989, Nuclear Instruments and Methods in Physics Research B, 42, 76
Mitler, H. E. 1972, Ap&SS, 17, 186
Mocchiutti, E. et al. 2003, in International Cosmic Ray Conference, Vol. 4, International Cosmic Ray Conference, 1809
Moskalenko, I. V., Strong, A. W., Mashnik, S. G., & Jones, F. C. 2003, in International Cosmic Ray Conference, Vol. 4, International Cosmic Ray Conference, 1917
Mueller, D., Swordy, S. P., Meyer, P., L'Heureux, J., & Grunsfeld, J. M. 1991, ApJ, 374, 356
Myers, Z. D., Seo, E. S., Abe, K., et al. 2003, in International Cosmic Ray Conference, Vol. 4, International Cosmic Ray Conference, 1805
Nicholls, J. E. et al. 1972, Nuc. Phys. A, A181, 329
Olson, D. L., Berman, B. L., Greiner, D. E., et al. 1983, Phys. Rev. C, 28, 1602
Osborne, J. L. & Ptuskin, V. S. 1988, Soviet Astronomy Letters, 14, 132
Palevsky, H., Friedes, J. L., Sutter, R. J., et al. 1967, Physical Review Letters, 18, 1200
Papini, P., Piccardi, S., Spillantini, P., et al. 2004, ApJ, 615, 259
Ptuskin, V. S., Moskalenko, I. V., Jones, F. C., Strong, A. W., & Zirakashvili, V. N. 2006, ApJ, 642, 902
Pulfer, P. 1979, PhD thesis, University of Bern
Putze, A., Derome, L., & Maurin, D. 2010, A&A, 516, A66
Putze, A., Derome, L., Maurin, D., Perotto, L., & Taillet, R. 2009, A&A, 497, 991
Putze, A., Maurin, D., & Donato, F. 2011, A&A, 526, A101
Ramadurai, S. & Biswas, S. 1974, Ap&SS, 30, 187
Ramaty, R. & Lingenfelter, R. E. 1969, ApJ, 155, 587
Rogers, J. G., Cameron, J. M., Epstein, M. B., et al. 1969, Nuclear Physics A, 136, 433
Seo, E. S. & McDonald, F. B. 1995, ApJ, 451, L33
Seo, E. S., McDonald, F. B., Lal, N., & Webber, W. R. 1994, ApJ, 432, 656
Seo, E. S. & Ptuskin, V. S. 1994, ApJ, 431, 705
Shalchi, A. & Büsching, I. 2010, ApJ, 725, 2110
Sourkes, A. M., Houdayer, A., van Oers, W. T. H., Carlson, R. F., & Brown, R. E. 1976, Phys. Rev. C, 13, 451
Strong, A. W. & Moskalenko, I. V. 1998, ApJ, 509, 212
Strong, A. W., Moskalenko, I. V., & Ptuskin, V. S. 2007, Annual Review of Nuclear and Particle Science, 57, 285
Tanihata, I. et al. 1985, Phys. Lett., B160, 380
Tannenwald, P. E. 1953, Physical Review, 89, 508
Teegarden, B. J., von Rosenvinge, T. T., McDonald, F. B., Trainor, J. H., & Webber, W. R. 1975, ApJ, 202, 815
Tripathi, R. K., Cucinotta, F. A., & Wilson, J. W. 1997, Universal Parameterization of Absorption Cross Sections, Tech. rep., NASA Langley Research Center
Tripathi, R. K., Cucinotta, F. A., & Wilson, J. W. 1999, Universal Parameterization of Absorption Cross Sections - Light systems, Tech. rep., NASA Langley Research Center
Trotta, R., Jóhannesson, G., Moskalenko, I. V., et al. 2011, ApJ, 729, 106
Tsao, C. H., Silberberg, R., Barghouty, A. F., & Sihver, L. 1995, ApJ, 451, 275
Usoskin, I. G., Alanko, K., Mursula, K., & Kovaltsov, G. A. 2002, Sol. Phys., 207, 389
Velichko, G. N. et al. 1982, Yad. Fiz., 35, 270
Walton, J. R., Heymann, D., Yaniv, A., Edgerley, D., & Rowe, M. W. 1976, J. Geophys. Res., 81, 5689
Wang, J. Z., Seo, E. S., Anraku, K., et al. 2002, ApJ, 564, 244
Webber, R. W. 1990a, in International Cosmic Ray Conference, Vol. 3, International Cosmic Ray Conference, 404
Webber, W. R. 1990b, AIP Conference Proceedings, 203, 294
Webber, W. R. 1997, Advances in Space Research, 19, 755
Webber, W. R., Golden, R. L., & Mewaldt, R. A. 1987, ApJ, 312, 178
Webber, W. R., Golden, R. L., Stochaj, S. J., Ormes, J. F., & Strittmatter, R. E. 1991, ApJ, 380, 230
Webber, W. R. & Rockstroh, J. M. 1997, Advances in Space Research, 19, 817
Webber, W. R. & Schofield, N. J. 1975, in International Cosmic Ray Conference, Vol. 1, International Cosmic Ray Conference, 312–317
Webber, W. R. & Yushak, S. M. 1983, ApJ, 275, 391
Xiong, Z.-H. et al. 2003, JHEP, 11, 048